12-2016

Linking nanoscale mechanical behavior to bulk physical properties and phenomena of energetic materials

Matthew R. Taw
Purdue University

Graduate School Form
30 Updated 12/26/2015

PURDUE UNIVERSITY
GRADUATE SCHOOL
Thesis/Dissertation Acceptance

This is to certify that the thesis/dissertation prepared

By Matthew Taw

Entitled
LINKING NANOSCALE MECHANICAL BEHAVIOR TO BULK PHYSICAL PROPERTIES AND PHENOMENA OF ENERGETIC MATERIALS

For the degree of Master of Science in Materials Science Engineering

Is approved by the final examining committee:

David F. Bahr
Chair

Jeffrey P. Youngblood

Steven Son

Teresa M. Carvajal

To the best of my knowledge and as understood by the student in the Thesis/Dissertation Agreement, Publication Delay, and Certification Disclaimer (Graduate School Form 32), this thesis/dissertation adheres to the provisions of Purdue University's "Policy of Integrity in Research" and the use of copyright material.

Approved by Major Professor(s): David F. Bahr

Approved by: David F. Bahr 11/29/2016
Head of the Departmental Graduate Program Date

LINKING NANOSCALE MECHANICAL BEHAVIOR TO BULK PHYSICAL PROPERTIES AND PHENOMENA OF ENERGETIC MATERIALS

A Thesis

Submitted to the Faculty

of

Purdue University

by

Matthew R. Taw

In Partial Fulfillment of the

Requirements for the Degree

of

Master of Science in Materials Science Engineering

December 2016

Purdue University

West Lafayette, Indiana

ACKNOWLEDGMENTS

I would like to acknowledge The US Air Force Office of Scientific Research for the funding of this project under grant number FA9550-16-1-0101 and Los Alamos National Lab for their collaboration. I would like to thank Dr. Bahr and his research group, Dr. Son, Dr. Carvajal, and Dr. Youngblood for their contributions and thoughtful insights. I also greatly appreciated the help of Vasant Vuppuluri and Mike Koppes in material handling.

I would like to thank my fiancée, family, and all my colleagues and the professors who encouraged me and helped me accomplish this work.

TABLE OF CONTENTS

Page

LIST OF TABLES iv

LIST OF FIGURES v

ABSTRACT vii

CHAPTER 1. INTRODUCTION 1
1.1 Background and Motivation 1
1.2 Energetic Materials 2
1.3 General Nanoindentation Methods 6

CHAPTER 2. VARIATIONS IN MECHANICAL RESPONSES OF ASPIRIN 9
2.1 Experimental Methods 10
2.2 Results 11

CHAPTER 3. THE MECHANICAL PROPERTIES OF MINIMALLY PROCESSED RDX 17
3.1 Abstract 17
3.2 Introduction 17
3.3 Experimental Section 19
3.3.1 Materials 19
3.3.2 Nanoindentation 19
3.4 Results and Discussion 21
3.5 Conclusion 26
3.6 Acknowledgments 27

CHAPTER 4. NANOINDENTATION OF ENERGETIC MATERIALS . . . 28
4.1 HMX 31
4.2 TATB 37
4.3 FOX-7 41
4.4 ADAAF 46
4.5 TNT/CL-20 Cocrystal 49
4.6 Trends and Drop Weight Sensitivity 53

CHAPTER 5. CONCLUSION 58

REFERENCES 61

LIST OF TABLES

Table Page

2.1 Hardness and Reduced Modulus of Aspirin 14

4.1 Mechanical Properties of Energetic Materials 53

4.2 Shear Stress at Yield in Energetic Materials 53

5.1 Comparison of Properties of Molecular Crystals 60

LIST OF FIGURES

Figure		Page
2.1	Arrays of indents on aspirin	11
2.2	Representative aspirin load depth curves	12
2.3	Aspirin residual indent impressions	13
2.4	Hertzian fit on elastic loading portion of an aspirin indent	14
2.5	Histogram of yield point loads for aspirin	15
2.6	Histogram of yield point shear stresses for aspirin	16
3.1	RDX residual indent impression	21
3.2	Representative RDX load depth curves	22
3.3	Box and whisker plot of reduced modulus of RDX crystals	23
3.4	Box and whisker plot of hardness of RDX crystals	23
3.5	Yield points in representative RDX load depth curves	24
3.6	Histogram of yield point loads in RDX	25
3.7	Cumulative fraction of yield point loads in RDX	25
3.8	Histogram of yield point shear stresses in RDX	27
4.1	Chemical structures of selected energetic materials	29
4.2	Images of all energetic materials crystals indented	30
4.3	Images of TATB crystals before and after removing a surface layer	30
4.4	Length and area of excursion illustration	31
4.5	Selected load depth curves for HMX	33
4.6	Box and whisker plots of hardness and modulus of HMX	34
4.7	Residual indent impression on HMX	35
4.8	Pop-ins observed in HMX load depth curves	35
4.9	Histogram and cumulative fraction of the loads at which the initial yield phenomena occurred in HMX	36

Figure Page

4.10 Histogram and cumulative fraction of the shear stresses at which the initial yield phenomena occurred in HMX 37
4.11 Selected load depth curves for TATB 38
4.12 Box and whisker plots of hardness and modulus of TATB 39
4.13 Residual indent impression on TATB 40
4.14 Low load behavior observed in TATB load depth curves 40
4.15 Histograms of the load and shear stresses at which the initial yield phenomena occurred in TATB 41
4.16 Selected load depth curves for FOX-7 43
4.17 Low load behavior observed in FOX-7 load depth curves 44
4.18 Residual indent impression on FOX-7 45
4.19 Box and whisker plots of the hardness and modulus of FOX-7 45
4.20 Selected load depth curves for ADAAF 47
4.21 Residual indent impression on ADAAF 48
4.22 Hardness of ADAAF crystals 48
4.23 Modulus of ADAAF crystals 49
4.24 Residual indent impression on TNT/CL-20 51
4.25 Selected load depth curves for TNT/CL-20 cocrystal 52
4.26 One load depth curve of each material 54
4.27 Excursion energy verse H_{50} 55
4.28 Excursion length verse H_{50} 55
4.29 Linearized excursion length verse H_{50} 56

ABSTRACT

MSMSE, Purdue University, December 2016. Linking Nanoscale Mechanical Behavior to Bulk Physical Properties and Phenomena of Energetic Materials. Major Professor: David Bahr.

The hardness and reduced modulus of aspirin, RDX, HMX, TATB, FOX-7, ADAAF, and TNT/CL-20 were experimentally measured with nanoindentation. These values are reported for the first time using as-received micron sized crystals of energetic materials with no additional mechanical processing. The results for TATB, ADAAF, and TNT/CL-20 are the first of their kind, while comparisons to previous nanoindentation studies on large, carefully grown single crystals of the other energetic materials show that mechanical properties of the larger crystals are comparable to crystals in the condition they are practically used. Measurements on aspirin demonstrate the variation that can occur between nanoindentation indents based on the orientation of a Berkovich tip relative to the surface of the sample. The Hertzian elastic contact model was used to analyze the materials initial yield, or pop-in, behavior. The length, energy, indentation load, and shear stress at initial yielding were used to characterize each material. For the energetic materials the length and energy of the yield excursions were compared to the drop weight sensitivity. This comparison revealed a general trend that more impact sensitive materials have longer, more severe pop-in excursions. Hot spot initiation mechanisms involving crystal defects such as void collapses and dislocation pile-up followed by avalanche are supported by these trends. While this only takes one aspect of impact sensitivity into consideration, if this trend is observed in a larger range of energetics these methods could possibly be used to great advantage in the early stages of new explosives synthesis to obtain an estimation of drop weight sensitivity.

1. CHAPTER: INTRODUCTION

1.1 Background and Motivation

Solid energetic materials, typically organic molecules with $C_wH_xN_yO_z$ chemical formulas, fall under the category of molecular crystals. Molecular crystals, almost exclusively organic crystalline materials, are composed of molecules held together by intermolecular dispersion forces and not by ionic bonds or covalent networks, distinguishing them from salts or metals [1, 2]. Many pharmaceuticals are also types of crystalline organics and the mechanical properties can be tested in similar manners to energetic materials [3]. For this reason being able to test the physical properties of organic molecular crystals is of great interest particularly to medical [3], military [4], and related fields of science. While the focus of this work is on energetic materials, with a very brief look at an example pharmaceutical, "organic" crystal is a rather broad category and there are many other applications that these types of materials are used for, such as photovoltaic devices [5, 6] and electronics [7]. Measured properties of energetics and pharmaceuticals can be qualitative or quantitive depending on the desired information. More qualitative mechanical properties of interest include compactibility and brittleness, as they affect the ability to press powders into tablets [8]. Quantitative properties of interest are modulus and hardness. Understanding the relationship between the structures of materials and how they affect these macroscopic properties has the potential to allow engineering of molecules that provide an optimal range of performance for various applications [9].

The large structural overlap between energetics and pharmaceuticals has made testing both types of materials with similar methods a common practice in certain studies [10]. Some substances, such as nitroglycerin serve in both roles, acting as a vasodilator (lowers blood pressure) and as the active ingredient in multiple explosive

formulations such as dynamite and smokeless gunpowder [11]. In testing and handling energetic materials, especially when synthesizing new and unknown materials, there are always associated risks and hazards. The sensitive nature of these explosives make even the safest environments and situations susceptible to unwanted accidents. The goal of this research is two-fold: first is to measure mechanical properties (hardness and modulus) of novel energetic materials, and of well characterized energetic materials in novel conditions. The second purpose is to look for correlations between elastic-plastic transition behavior and impact sensitivity. This idea, discussed further later, is based on several mechanisms for hot spot initiation after impact that include heating at dislocation pile-ups or other crystal defects, to which the precursor is dislocation generation and movement [12]. Subsequent dislocation avalanches may then be responsible for explosive behavior. If dislocation behavior and energy release can be observed in deformation then there may be a quantifiable relation between that energy release and impact sensitivity. This could potentially lead to a faster, safer, and more cost efficient method of testing new energetic materials.

1.2 Energetic Materials

Since the time nitroglycerin was first commercialized by Alfred Nobel mid 19th century there has been a great need to improve the safety of explosives in their manufacturing, handling and storage. Alfred Nobel himself realized this when a nitroglycerin explosion accident killed his brother and several other workers in 1864. This spurred him on to make the more stable explosives, and one of the results of his work ended up being dynamite. There have been countless explosive accidents throughout history in nearly every capacity they are used, while not comprehensive Ramsay offers a systematic list of 116 recorded accidents over the course of 50 years at Los Alamos National Lab alone [13]. The overall challenges involved in explosive safety are described by Ek:

> "Whatever method we use to predict possible accidents, we have one fundamental problem. The substances can be subjected to so many different

> situations, each with its own pattern of different kinds of stresses, that it is impossible to imagine them all. With more understanding, we can make predictions of risks in more and more situations, but a wholly complete understanding and description of all potential risk situations will never be possible." [14]

Even today this is this is still a fundamental problem, just recently the SpaceX Falcon 9 rocket exploded on launch September 1, 2016, where they believe the issue was a problem with the propellant, though the cause is still unknown. Thankfully no one was hurt in this event, however there is evident need to improve these materials, and many resources are going into that effort.

Energetic materials contain both fuel and oxidizer on the same molecule, this allows then to combust rapidly even in the absence of additional oxidizer. Their reactions are highly exothermic and temperature dependent. Commonly they are divided in to three categories: pyrotechnics, explosives, and propellants, though often times these categories can overlap with each other as explosives can be used in propellants and pyrotechnics and vice versa. High explosives can be further classified based on their sensitivity as primary, secondary, or tertiary. Primary explosives, such as lead azide, are the most sensitive towards shock, thermal, or other initiation mechanisms and often used as primers to detonate other charges. Secondary explosives are less sensitive in these regards but have high energy densities, explode violently, and are typically the major components in explosive charges. Materials of interest in this study include the secondary explosives RDX, HMX, TATB and other less common energetics. Tertiary explosives are the least sensitive, though they can detonate in the right conditions, and are mostly oxidizers such as ammonium nitrate and ammonium perchlorate. Each type of explosive has its own uses, but in general two key desires are lower sensitivity to prevent unwanted detonation and higher energy density and performance capabilities. Other factors of consideration are the life span of energetic materials, how to disarm them, and how can they use non-toxic or greener materials to prevent health hazards [15].

There are a multitude of experiments done to test the sensitivity of an energetic material. As mentioned, no single test is an adequate qualifier of the safety of a material because there are countless stimuli that can cause a material to detonate, whether through shock, friction, thermal activation, static electricity or other causes. Each type of sensitivity test looks at a different impetus that a material may be susceptible to that could cause it to either deflagrate or detonate. There are also many tests for explosive behavior, detonation properties, chemical behavior, mechanical behavior, flame characteristics and a variety of other aspects related energetic materials. The different sensitivity test give knowledge about one very specific type of stimulus a sample may be subject to, so a plethora of tests must be done in order to understand overall properties, procedures, and cautions needed with any given material.

All tests done on explosives are statistical in nature and may provide different results if tests are done in different machines due to different configurational set-ups, though trends in data are consistent [16]. This can make using comparisons between sets of data that come from different locations difficult to draw quantitative conclusions from even when tests are done using standard procedures. It also means that a large amount of material must be prepared in order to obtain results of any meaning. For instance, in drop weight impact tests (such as those using a BAM Impact apparatus) a weight, usually between 1 and 10kg, is dropped onto a sample to see if it detonates. The mass of sample tested can vary but in the smallest apparatuses the amount tested is on the order of milligrams [16]. The drop height, H_{50}, is determine by the height at which 50% of the samples detonated. At lower heights if the material is less sensitive, then after a given number of tests it is possible none will detonate. As the height of the weight is increases maybe a two out of ten will detonate. Then once a certain height is reached all samples tested at that height will detonate. The middle height, when half of the samples detonated and half did not is the recorded value. This number represents a distribution that may be rather broad for a given explosive, indicating that a material can be sensitive to a large range of mechanical impacts.

However testing methods such as this are very time consuming and require lots of material. For drop weight impact testing alone a sample may be tested tens of times at each height for a multitude of heights, which can easily result in a very large number of tests for best results. This takes time as, new explosives in particular, are synthesized in small quantities on the gram scale before they can be made on larger scales. While each test may only take several milligrams, a number of tests done can quickly add up to larger amounts. Not only must materials be synthesized for impact tests, but also for each type of test to be performed since these methods are destructive. The time and money invested increase for each test performed as each test is vital in providing necessary information. Another cost concern in testing explosives is the wear on the instruments. Many apparatuses have mounting blocks, tubes, or other pieces that are designed to hold or impact the explosive. During detonation these pieces can be dented as a natural course in the testing process because of detonation shock waves. This requires replacement of parts that are many times single-use when testing detonation properties as there are few "non-destructive" tests available when testing explosives.

During impact tests the formation of "hot spots", localized regions in a material that are heated to a much greater temperature than the surroundings, is seen as the mechanism of how detonations occur [12]. If the size, temperature, and during of the hot spot meet certain conditions, in other words form a critical hot spot, then they can propagate a shock wave causing detonation. If these conditions are not met then the hot spot quenches. Multiple mechanisms for hot spot formation have been proposed, a list and summary of the most widely accepted mechanisms is given by Field et al. in the given reference [17]. Several of these mechanisms involve hot spot formation from: collapse of voids or cavities, adiabatic shear and shear banding, and dislocation pile-ups followed by avalanches. According to Field the role of dislocations and dislocation pile-up on its own does not seem to generate enough heat to ignite a sample, however multiple mechanisms may be act work simultaneously towards hot spot activation and can have additive affects. This leads to the rather interesting

question of what is the role of dislocations in hot spot formation and if observing dislocation behavior can in any way allow the prediction of impact sensitivity.

Being able to understand and measure more fundamental properties, such as dislocation nucleation and behavior, of energetic materials is necessary when looking at models and mechanisms for hot spot initiation. The fundamental measurements themselves are valuable knowledge to the scientific community but can also be used to provide supporting evidence for these proposed mechanisms. Sensitivity in drop weight impact tests has been shown to depend on a large number of factors, some of which are particle size [18], morphology [19], surface roughness [20] and processing method [21]. Looking at specifically dislocation behavior as one factor for hot spot initiation may be useful in validating mechanisms such as dislocation pile-up, but cannot provide a comprehensive picture of all causes for impact sensitivity. It would be an oversimplification to assume that by measuring the modulus, hardness, and looking at dislocations the impact sensitivity of a material will solely depend on these parameters, however they can provide valuable insight to the process occurring. Even if it is found that there is little or no relation between the dislocation behavior and sensitivity, by measuring these physical quantities a larger general understanding is developed for the materials currently being used and worked with.

1.3 General Nanoindentation Methods

Nanoindentation has become a common method of testing molecular crystals as it can measure useful mechanical properties, primarily hardness and reduced modulus [9], however it can also be used to observe slip systems [22], phase changes and dislocation activation [23], polymorphs and anisotropy [24], fracture [25], and other types of useful information. As will be discussed in more detail in the following paragraphs, by using Hertzian elastic contact models and observing load-depth curve pop-in behavior the elastic-plastic transitions, energy released in transition, onset of plastic deformation, and shear stresses in the elastic region can be observed [26]. This allows for a study of the dislocations and elastic-plastic transitions in energetic

materials that may then correlate to the impact sensitivity of the material through the described hot spot initiation mechanisms of dislocation pile-up.

Nanoindentation is a method where a tip with a known geometry is indented into a surface and withdrawn while measuring the force and displacement. From this information a load-depth curve is generated which can be analyzed to give a variety of mechanical properties. Oliver and Pharr describe a method using the load-depth curve to determine the hardness and reduced modulus of a sample [27]. The unloading slope of the load-depth curve is equal to the stiffness of the sample, S, and can then be used to calculate the reduced modulus E_r by

$$E_r = \frac{S\sqrt{\pi}}{2\beta\sqrt{A}}, \tag{1.1}$$

where β is a tip geometry constant that is approximately unity and A is the contact area measured using the tip area function. The hardness of the sample is calculated by the maximum load divided by the contact area,

$$H = \frac{P_{max}}{A}. \tag{1.2}$$

For the loading portion of the load-depth curve the Hertzian elastic contact model is an appropriate description of the initial elastic behavior [26]. The elastic portion of the loading can be fit to the equation

$$P = \frac{4}{3}E_r\sqrt{R\delta^3}, \tag{1.3}$$

where R is the tip radius and δ is the indentation depth. Following the Hertzian model the maximum shear stress that the surface experiences at a given load can be calculated from

$$\tau_{max} = 0.31\left(\frac{6E_r^2}{\pi^3 R^2}\right)^{1/3} P^{1/3}. \tag{1.4}$$

Using this equation the shear stress at given points or features in the elastic portion can be found quite easily. Often, if a sample exhibits elastic behavior, the

transition to plastic deformation is seen in the load depth curve as a sudden jump in displacement (in depth-controlled experiments), also called a "pop-in", as there is a large rapid movement of dislocations [28], though this isn't always the case [29].

There are several challenges with nanoindentation, particularly for energetic materials, but also to achieve best results in general. The materials of interest, namely secondary explosives, tend to be powder crystalline samples. In order to obtain accurate and consistent data the sample surface to be indented must be level. The errors introduced in calculated values become significant when samples are tilted by more than a few degrees [30]. This issues becomes more apparent the smaller the sample is as it becomes harder to not only find suitable surfaces but to orient them properly for indentation. The most common method of overcoming this obstacle is to synthesize large single crystals with well behaved surfaces that can be easily manipulated and aligned. This however introduces the question, do large carefully grown samples accurately reflect properties of the material in its as-used state [21]? Secondly, not all materials can be grown as large crystals and morphological modifiers are sometimes added to increase the stability of the crystal [31]. In this case it is no longer a pure sample being tested, and the properties measured may reflect the impurities added. Another method to try and deal with small crystals is to embed the crystals in a binder, usually a polymer matrix, then polish the surface so that the smaller crystals are exposed [32]. The problem with this method is that the binder may influence the elastic properties measured during indentation because the binder itself is flexible, and the polishing may alter surface conditions. Similarly, surface roughness can adversely affect results if the roughness is on the same order of magnitude as the indent size. This is usually overcome again by polishing the sample, however polishing has been shown to influence the surface dislocations present which can alter the surface properties [33]. Overcoming these present experimental limitations is a key factor in being able to test materials that previously could not be experimentally tested, instead relying on simulations to predict these mechanical properties.

2. CHAPTER: VARIATIONS IN MECHANICAL RESPONSES OF ASPIRIN

There are many examples of using nanoindentation to study pharmaceuticals in the literature [3, 21, 34, 35]. Mechanical properties of acetylsalicylic acid, or aspirin ($C_9H_8O_4$ monoclinic, $P2_1/c$ space group [36]), have been studied using indentation methods since as early as 1969 [37], and indentation methods continue to be an effective method in improving existing information and providing new information on aspirin. More recent studies have used nanoindentation to study aspirin single crystals [24, 38] as well as compact tableted aspirin [39]. In the aforementioned studies, Varughese et al. measured the hardness and modulus of different faces to distinguish between two different polymorphs of aspirin, while Olusanmi et al. reports the hardness and modulus of multiple faces. The reported hardness and reduced modulus for the (001) faces of aspirin ranges from 0.11-0.240GPa and 2.81-9.57GPa respectively. Similarly for the (100) faces the values range from 0.11-0.28GPa and 4.73-7.16GPa, while other types of study give values in between these [40].

An important consideration in any indentation experiment is the type of tip that is used. Tips of different geometries such as spherical indenters, flat punches, Berkovich, cube-corner, Vickers, and Knoop indenters, have different symmetries. The Berkovich tip, which was used by Varughese and Olusanmi, is one of the more common ones which has threefold symmetry as its general shape is that of a triangular pyramid. This means that when the Berkovich tip indents a surface the orientation of the surface relative to the symmetry lines of the tip may differ. This can cause different localized stresses as the indenter load is distributed along different axes depending on how the surface is indented. Given the three-fold symmetry of the Berkovich it stands to reason that indents done where the tip is rotated by 120^o increments should give identical results. However for indents where the tip is "in-

between" these angles, for instance if an indent is done on a surface then the surface is rotated clockwise 90^o in-plane, the resulting measured mechanical properties may be different. By indenting a single face of single crystal aspirin at rotating the sample the magnitude of the differences in measurements based on the orientation of the tip relative to a given surface will be investigated.

2.1 Experimental Methods

The mounting procedure described by Maughan et al. [41] for sub-millimeter crystals was used for preparing all samples. Even though the aspirin crystals were millimeter sized and could be easily manipulated with tweezers this method was still used in order to verify that it could be used successfully. This mounting method was subsequently applied to much smaller crystalline powders that are discussed in later chapters. In this procedure a small crystal is placed on a clean aluminum block that rests on a scissor jack. In well faceted samples a flat surface will be in contact with the aluminum block as gravity pulls the crystal into a stable position. A stand is used to hold a magnet above the sample. Then a steel disk with an applied adhesive is attached to the magnet with the adhesive facing downward towards the sample (if the magnet is too strong and makes the disk difficult to remove then a spacer such as a thin piece of wood or plastic can be placed between the magnet and the disk). For all samples, unless otherwise noted, the adhesive used was Crystalbond 555 applied to the steel disk after heating the disk on a hot plate to $100\,^o$C. The scissor jack is then used to raise the crystal until it comes into contact with the adhesive. Once the crystal has bonded to the adhesive the disk is removed from the magnet and flipped over so the sample and the surface originally in contact with the aluminum is facing upward. The smaller the crystals used the more difficult it becomes to successfully mount them. An important reminder for this technique is to ensure that the aluminum block and the steel disk attached to the magnet are parallel, if this is not the case the sample will undoubtedly not be suitable flat.

Nanoindentation of the aspirin samples was done with a Berkovich tip in a Hysitron 950 Triboindenter. The quasi-static indents were performed in an open-loop rather than depth or load controlled. The load function contained a 5 second linear loading segment to a maximum load of 5000μN, a 5s hold at the peak, followed by a 5s linear unload. Several low-load quasi-static indents were done with similar load functions however the maximum load ranged from 50-100μN. Partial-unload indents contained 7 load/unload segments, also to a maximum load of 5000μN. Multiple low-load and partial-unload indents were performed. On a single crystal, to test the variation caused by tip orientation relative to the sample surface, four "tip angles" were chosen to indent the surface at. An array of 9 indents was done on the aspirin crystal, then the sample was rotated clockwise in-plane a given amount and the 9 indents were repeated. This was done for the four different angles of rotation, post-indent images were used to verify the rotation amount between each array of indents. The initial set of indents was considered to be done at 0 degrees, and the amount of clockwise rotation of the sample from that initial position is θ, the recorded angle.

2.2 Results

The angles to which the surface was rotated clockwise relative to the tip were 0, 15, 50, and 83^o, with zero being the initial indent position. The spacing bewteen indents in each array was 30μm. Nine indents were done at each angle, the arrangements of the indents are given in Figure 2.1.

Figure 2.1. The arrays of 9 indents at different angles, the rightmost being zero degrees with increasing angle to the left.

In Figure 2.2 a representative load-depth curve is given for each position. The load-depth curves have slight variations in the location and severity of pop-ins, however the overall shape and curvature of each indent is very similar with the exception of the indents done at 83^o. This indent has a shallower slope and slightly greater penetration depth, indicative of a softer surface.

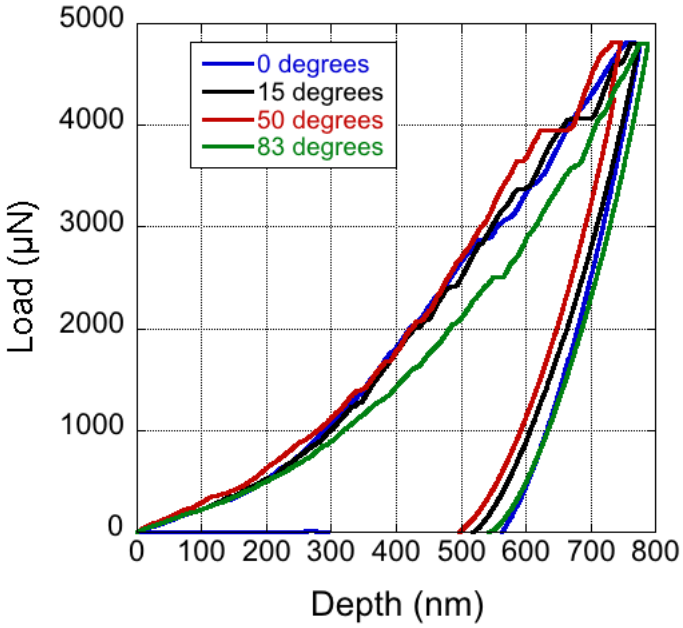

Figure 2.2. Representative load-depth curves of each angle indented in aspirin.

A residual indent impression of each angle is given in Figure 2.3, each image has been rotated so that it represents the actual orientation of each indent relative to the other in space. The lines that can be seen bisecting each indent could possibly be identical slip bands as they all lie in nearly the same direction on the crystal surface. Further studies would need to be conducted to confirm this. There did not appear to be any cracking in the aspirin surface. From the load depth curves of each indent the average H and E_r values at each position were calculated and recorded in Table 2.1.

There is not a significant change in properties for the first three angles as the hardness and reduced modulus are statistically the same. Statistical analysis was done using the Wilcoxon rank sign test for paired data sets. P-values were obtained

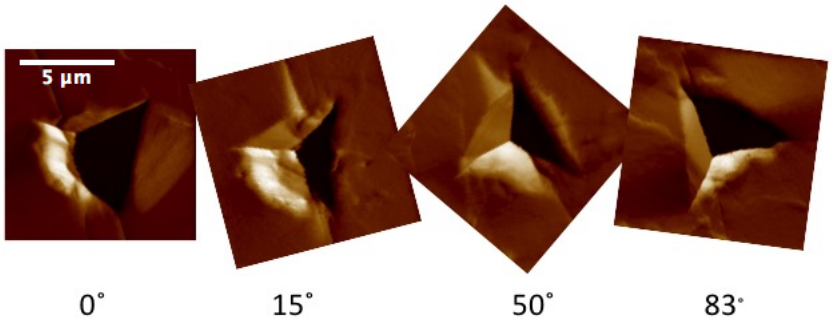

Figure 2.3. Residual indent impressions on aspirin at 0, 15, 50 and 83^o. This and all following indent impressions are gradient images giving the slopes of the surface.

comparing the data sets of hardness and modulus for each angle to all other angles, if the P-value was less than 0.05 the data sets were considered statistically different. The data from indents done at 83^o when compared with other angles gave a P-value of 0.0039 for hardness and 0.020 for modulus. P-values for comparisons of the data at 0, 15, and 45^o to each other showed statistical equivalence according to this model with values of 0.055 and greater. Indents done at 83^o show a decrease in both H and E_r just as in the load-depth curve deeper indents were observed. This is possibly because the stress distribution caused by the loading with this particular arrangement is more favorable for slip on the surface indented. This would decrease the energy required for plastic deformation making the surface appear softer. The modulus of aspirin given here falls exactly in the range of values reported by Varughese and Olusanmi, however the hardness is slightly higher. This is reasonable as the modulus is a material property, while the hardness, though closely related is a measure of a mechanical response that can be influenced by factors such as the bluntness of the tip used. The differences in tip orientation relative to the surface may not be significant in some cases but as can be seen in Table 2.1 may be the cause of up to a 8% difference in property values as was the case with indents done at 83^o. This may be one contribution to some of the discrepancies in values reported in the literature.

Table 2.1.
Hardness and Reduced Modulus of Aspirin

θ **(degrees)**	**H(GPa)**	E_r**(GPa)**
0	0.32±0.01	7.2±0.6
15	0.32±0.03	7.4±0.9
50	0.34±0.03	7.4±0.6
83	0.28±0.02	6.8±0.4

It has also been noted by both Varughese and Olusanmi that load-depth curves of aspirin contain multiple pop-ins or displacement bursts, particular on the (100) face. Using the Hertzian contact model and equation (1.4) the shear stress at which the initial pop-ins occur was calculated. Figure 2.4 demonstrates the elastic contact portion of a low-load indent showing that equation (1.3) is an adequate model for the elastic behavior of aspirin.

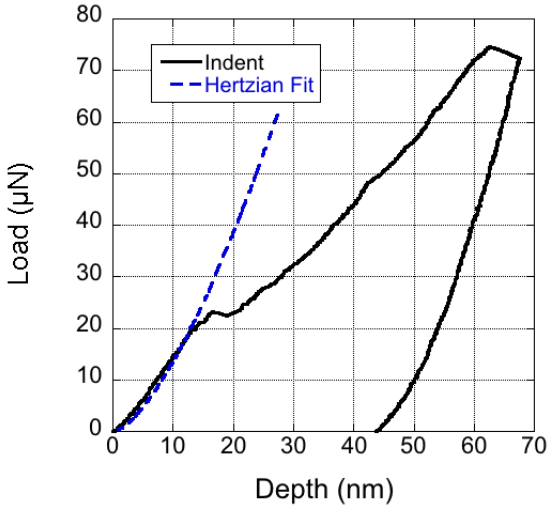

Figure 2.4. Example Hertzian fit to the elastic loading portion of an indent done in aspirin.

The first pop-in, or yield point, can be seen at approximately 15nm where the load-depth curve begins to deviate from the Hertzian fit. The load where this occurs is 23μN, and from (1.4) the shear stress is 0.11GPa where the this event occurred. An additional 21 low-load indents were done to observe the yield point behavior. Indents with less than 1000μN loads were used instead of the 5000μN indents used previously as they provide better resolution in the desired regions. Figure 2.5 and 2.6 give a histograms of the loads and shear stress at which the pop-in yield point occurred for each of these indents. The average shear stress to cause plastic deformation in aspirin is 0.95GPa.

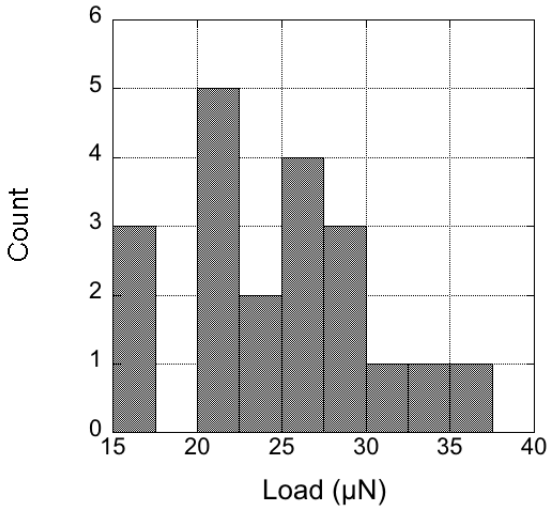

Figure 2.5. Histogram of the loads where initial pop-in phenomena occur in all indents done on aspirin.

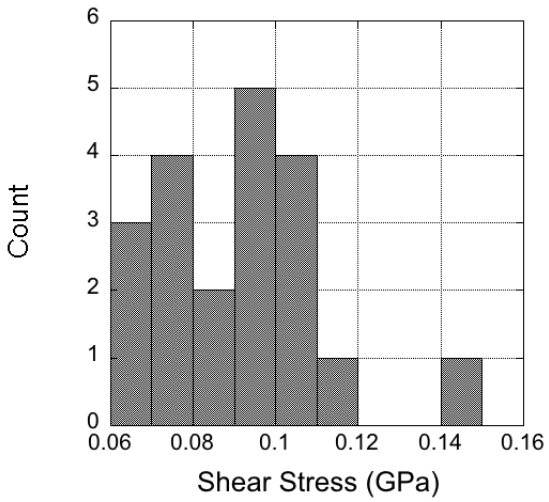

Figure 2.6. Histogram of the shear stress where initial pop-in phenomena occur in all indents done on aspirin.

3. CHAPTER: THE MECHANICAL PROPERTIES OF MINIMALLY PROCESSED RDX

This chapter has been submitted for publication to Pyrotechnics, Explosives, and Propellants and is currently under review.

3.1 Abstract

We report for the first time the mechanical properties of RDX crystals in a conventionally processed, sub-millimeter form that have had no additional mechanical processing. Nanoindentation of RDX powders was used to measure the elastic modulus (19.1±1.9 GPa), hardness (0.741±0.098 GPa), and yield point (onset of plastic deformation) on the as-grown faces of seven different RDX crystals, selected to provide random orientations. Properties within each crystal showed narrow distributions while the range of properties across all crystals is indicative of testing a variety of orientations. The elastic modulus and hardness are within the range of other published reports on bulk and mechanically polished RDX. The distribution in yield point behavior, with the onset of plasticity occurring between 0.1 and 0.7 GPa, indicates that powders of RDX likely contain a significant number of dislocation sources in the as-processed condition, suggesting that deformation sources are prevalent in the energetic component of plastic bonded explosives prior to incorporating into pressed forms.

3.2 Introduction

The mechanical response of energetic materials, particularly the transition between elastic and plastic deformation, may impact the overall sensitivity of the material [4,18]. Small scale mechanical testing, such as instrumented indentation methods

commonly referred to as nanoindentation, are a convenient method to probe both elastic, plastic, and fracture behavior of solids. There are many examples in the literature of using indentation techniques on molecular crystalline solids (broadly encompassing energetics, pharmaceuticals, and foods) to assess the general hardness [34], elastic modulus [21] including elastic anisotropy [35], the activation and identification of specific slip systems [22], contact fracture [25], and the onset of plastic deformation.

One fundamental challenge in any mechanical test is the balance between assessing properties in the "as used" conditions, and the need for sample preparation that could influence the resulting properties. In particular, the stress needed to initiate plastic deformation in a solid has two main components; there is a stress needed to nucleate dislocations in a dislocation free solid, and there is a stress required to activate an existing dislocation source [23, 33, 42, 43]. The former is often discussed as the theoretical strength of a solid, while the latter must consider the existence of prior dislocations.

There is strong evidence that defects within crystalline RDX (cyclotrimethylenetrinitramine) are related to shock sensitivity [44, 45]. As plastic deformation in energetic materials relies upon a limited number of slip systems [4, 46] it has been suggested that the onset of plastic deformation may be one of the processes needed to initiate a "hot spot". Observing plastic deformation behavior and dislocation density in energetic crystals may give insight as to the degree such mechanisms influence shock sensitivity. Existing studies of the mechanical response of RDX, and many molecular crystals in general, are somewhat limited, but are broadly separated into two categories. First, testing well characterized carefully grown and curated single crystals of specific orientations allows for fundamental studies of the material?s properties. However, one open question is then how representative are these crystals to the crystalline forms used in practice; which are grown at different rates and subjected to more (or different) mechanical stresses such as milling, grinding, or compaction. The second type of test is to assess small crystals in their form used in service (i.e. small, sub-mm crystals). In many cases this requires mounting and polishing the samples

in a binder [32, 47] or in the case of some pharmaceuticals in tableted form [8]. This paper will address the question of similarity in mechanical response between large, carefully grown and curated crystalline forms of RDX to those of minimally processed individual small crystalline forms of the same chemistry. The mechanical properties of interest will be elastic modulus, hardness, and the stress needed to nucleate dislocations, and both averages and distributions of properties will be presented.

3.3 Experimental Section

3.3.1 Materials

Crystals used for nanoindentation were as received Type II, Class III RDX crystals from BAE. The largest dimension of the crystals was about 0.5mm and the crystals were mounted on 1cm diameter steel disks using the procedure described by Maughan et al. for sub-millimeter crystal mounting [41]. An optical microscope was used to confirm that a suitable flat surface with an area large enough for indentations was present. The surface tilt was determined by sweeping the field of view in an optical microscope across the sample and focusing it with a micrometer on the desired regions to determine the height profiles. Ideally the surface to be indented would be completely level, however small tilt angles have been shown to not significantly impact hardness and reduced modulus by more than a few percent [30]. Samples that were tilted less than 4° were considered acceptably flat for indentation. Post-indentation atomic force microscopy (AFM) images using the indenter tip were also used to confirm that all surfaces were tilted less than 4°.

3.3.2 Nanoindentation

Nanoindentation was done in a Hysitron 950 TriboIndenter with a low load (quasi-static mode) QSM transducer. All indents were performed using a Berkovich tip. Quasi-static single indents were done with linear loading rates reaching a peak force of 1mN in 30s followed by a 5s hold at the peak force and a 5s unload. The

longer load times were to ensure that all features, particularly load excursions or "pop-ins", of the load depth curves were clearly visible and distinct. These load excursions are the characteristic rapid jumps in displacement at a given load seen at various locations in load depth curves. The initial load excursion can be a sign of an elastic-plastic transition and has been postulated to be a function of local dislocation density [42]. Slower loading rates allow this elastic-plastic transition to be clearly identified in the load-depth curves by making pop-in discontinuity occur over a larger depth range. In-situ AFM imaging was done prior to indentation to ensure that areas to be indented did not contain any abnormal surface features that would negatively impact results.

After mounting approximately 20 crystals, 7 unique RDX crystals that met the minimum tilt and macroscopic flaw free conditions were selected for indentation, 6 indents were done on each of the first two crystals (RDX1 and RDX2) and 8 indents done on each subsequent crystal. All indents had at least 20μm spacing from any given edge or previous indent. Additionally, several indents with maximum loads ranging from 15 to 30μN were performed to determine if the initial loading was indeed elastic and not indicative of some plasticity prior to a pop-in. All low load tests did not exhibit load excursions and confirmed that loading prior to the pop-ins was purely elastic, as opposed to exhibiting plastic deformation prior to a significant yield point [29]. The loads used were sufficiently low that no cracking was present in any of the samples after indentation. A scanning probe microscopy image of a residual impression from an indent is given in Figure 3.1 to demonstrate that no evidence of indentation-induced cracking in the RDX was found in this study.

The hardness and reduced modulus of RDX were calculated using the method described by Oliver and Pharr given in the introduction. The hardness was determined from equation (1.2) where, A, is the contact area as a function of depth. The contact area function is based on prior calibration of the tip area in fused quartz. From the initial slope of the unloading curve, using equation (1.1) the reduced modulus, E_r, was calculated.

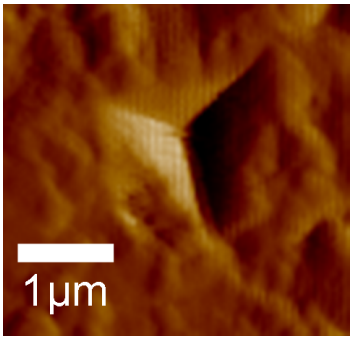

Figure 3.1. Scanning probe microsocpy image of a 1 mN indentation impression in RDX using a Berkovich tip. No indentation induced cracking was seen for any indent in this study; the loads used were well below the fracture strength of RDX.

3.4 Results and Discussion

Representative load-depth curves are given in Figure 3.2 showing common behavior for the indents on RDX crystals. The average reduced modulus and hardness over all 7 randomly oriented crystals were 19.1±1.9GPa and 0.741±0.098GPa respectively. The reduced modulus of each individual crystal is given in Figure 3.3. These values are in good agreement with previous studies that have reported reduced modulus and hardness values for large RDX single crystals [48, 49] and small RDX crystals embedded in a polymer resin [47]. The reduced modulus of the randomly oriented small crystals is fairly uniform, with the exception of crystal RDX7, and fall in the range of 16.2GPa and 21.0GPa reported by Ramos [48] for the (001) and (210) faces indicating that multiple faces that were indented on the small crystals giving an average between the maximum and minimum values. The reduced modulus of RDX8 was slightly higher than the other crystals and is closer to Weingarten and Sausa's [49] reported reported value of 22.9GPa for the (210) face. All of the previously listed results are slightly higher than resin embedded RDX crystals studied by Hudson [47] which have reduced moduli ranging from 15-17GPa, depending on the defect density.

The hardness of each RDX crystal, given in Figure 3.4, is centered around two different values. Three of the smaller RDX crystals had a hardness value near

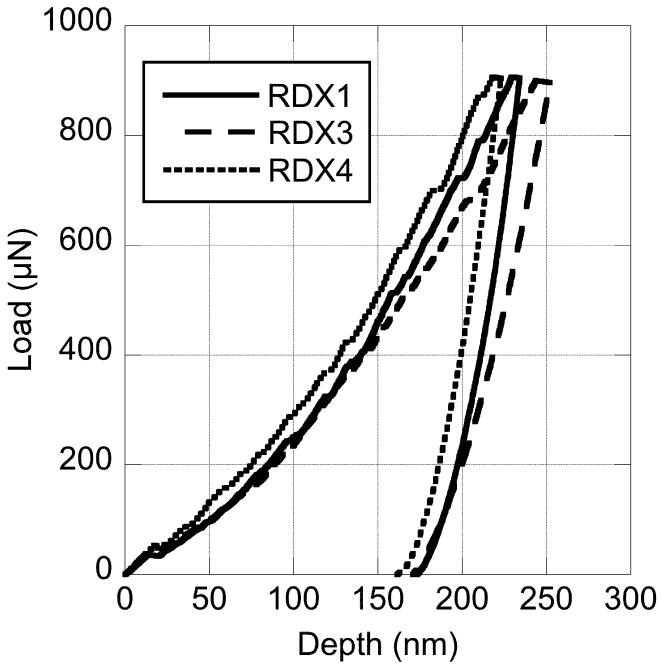

Figure 3.2. Representative load-depth curves of indentations into BAE Type II Class III RDX crystalline powder samples.

0.6Gpa, which is very similar to 0.61GPa report by Ramos for the (001) face. The other four RDX crystals had hardness values near 0.85GPa, much harder than the largest reported value by Ramos of 0.68Gpa for the (021) face and closer to the 0.798GPa value reported by Weingarten and Sausa for the (210) face.

The low load portion of selected load-depths curves are shown in Figure 3.5 highlighting the yield point where the elastic-plastic transition occurs. While the critical material property is the applied pressure, not the load, it is worth noting that with similarly shaped indenter tips the load excursions observed in this current study are similar to those that have been observed previously for the (210) face of RDX [49], having observed yielding at loads between 55 and 65μN. A distribution of all loads at which yield points occur is given in Figure 3.6 and a plot of the cumulative fraction of yield points that occurred is given in Figure 3.7. The shape of the cumulative plot in Figure 3.7, with a large tail at the higher end of the load spectrum, shows

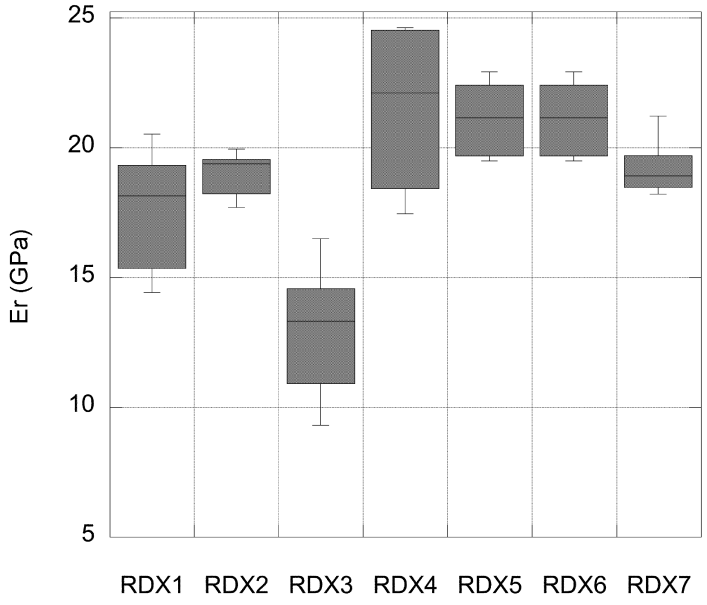

Figure 3.3. Box plot showing the median, upper and lower quartile, and total range of reduced modulus measured for each crystal.

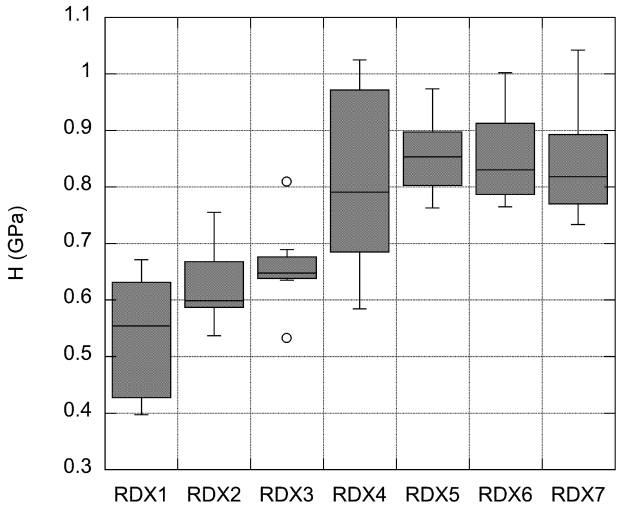

Figure 3.4. Box plot showing the median, upper and lower quartile, and total range of hardness measured for each crystal.

similar behavior to thermally and mechanically cleaved large RDX crystals; this case in which the median is lower than the mean and there is a tail at higher loads is likely a result of higher dislocation or defect density leading to lower yield points as sources are activited rather than nucleated in pristine material [42]. This suggests that there are a significant number of defects in as-processed RDX, comparable to those present in large single crystals of RDX that had dislocations introduced into the system through a cleaving process.

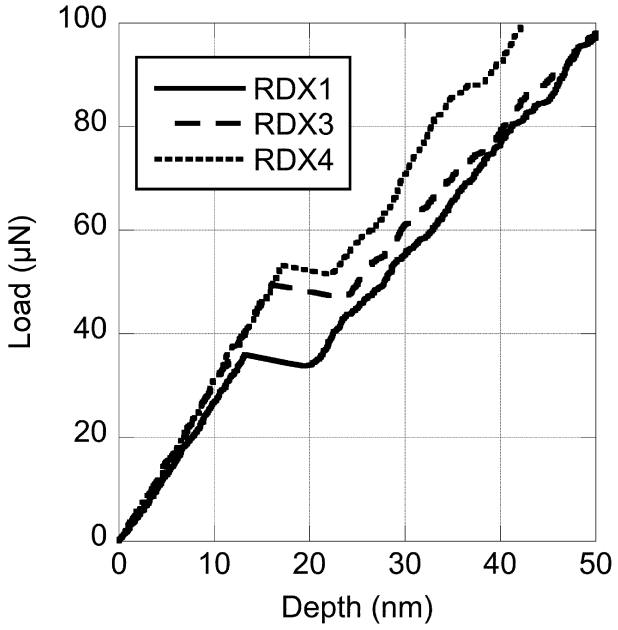

Figure 3.5. Elastic-plastic transition seen as load excursions at 37, 50, and 53μN in the initial loading portion of the same load-depth curves given in Figure 2. Load excursions of this nature were clearly visible in all crystals occurring at loads between 20 and 70μN

In order to determine the shear stress at which pop-ins occurred the initial loading slope in the elastic region was fit to a Hertzian contact model. The Hertzian model assumes elastic contact between a spherical indenter and an infinite half space and can be used to effectively represent the initial elastic loading segment during nanoindentation [26]. From the model an effective tip radius R can be obtained knowing the load, P, depth δ, and elastic modulus measured from the latter portion

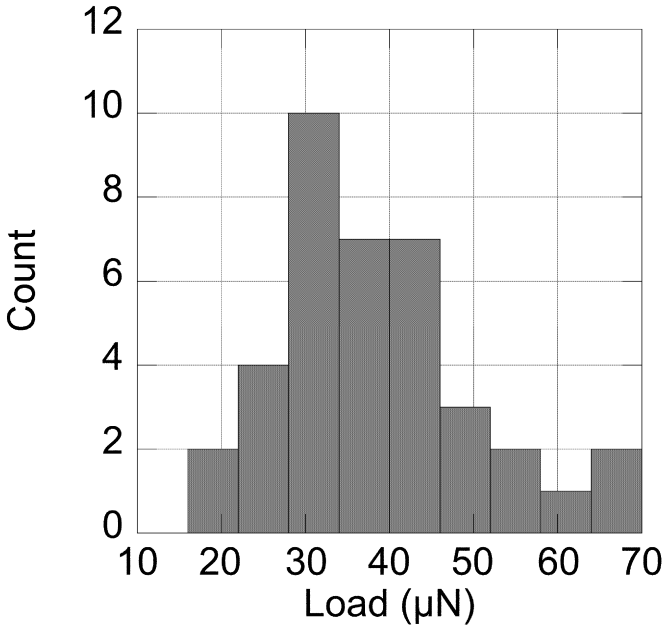

Figure 3.6. Histogram of loads at which the initial yield point occurred in all tested RDX crystals.

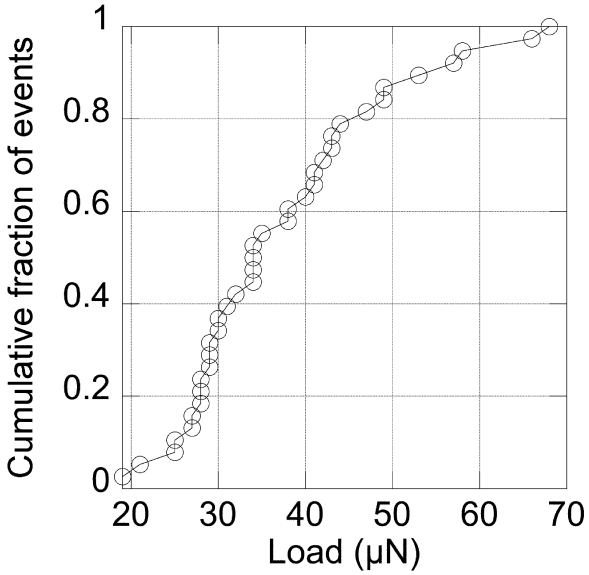

Figure 3.7. Cumulative fraction of yield point excursions that occurred in all tested RDX crystals as a function of load.

of the load-depth curve by equation (1.3). The tip radius was determined individually for each crystal indented. This was done because the conditions of each individual crystal may differ from the assumptions made in the Hertzian model. Prior studies have demonstrated that the local tip radius extracted from an indentation can vary by up to 20% from the tip radius measured using atomic force microscopy [50], and so the concept of using a local measurement for each indentation to account for variations in the surface is defensible. Using the tip radius the maximum shear stress under the indenter tip is found with equation (1.4).

A histogram of the shear stresses at which the elastic-plastic transition occurs is presented in Figure 3.8. The shear stresses at which yield points occur for each crystal indicate that there is a fairly broad distribution of crystal strength while the other mechanical properties remain relatively uniform. The calculated shear stress values are slightly lower than the 0.4-1.0GPa range reported by Ramos and are between 1/10 and 1/100 of the reported shear modulus of 5.75-9.26GPa [51]. The higher values would indicate dislocation nucleation, while shear stresses below about 1/30 of the shear modulus would suggest an alternative path such as activation of existing dislocations [26,43,52]. The range of shear stress values indicates that both dislocation activation as well as nucleation may occur depending on the existing defects in each individual crystal.

3.5 Conclusion

This paper has demonstrated that the mechanical properties of sub-mm RDX crystals can be measured using nanoindentation with minimal processing requirements, and the elastic properties measured are comparable to bulk material forms of RDX. Since surface preparation methods such as mechanical polishing or cleaving can impact the near surface deformation modes, and alter both the mean and distribution of the onset of plasticity, being able to test as-fabricated materials enables both assessment of materials at various stages of processing and/or aging, as well as rapid screening of new materials without the need to grow mm- to cm-scale single crystals.

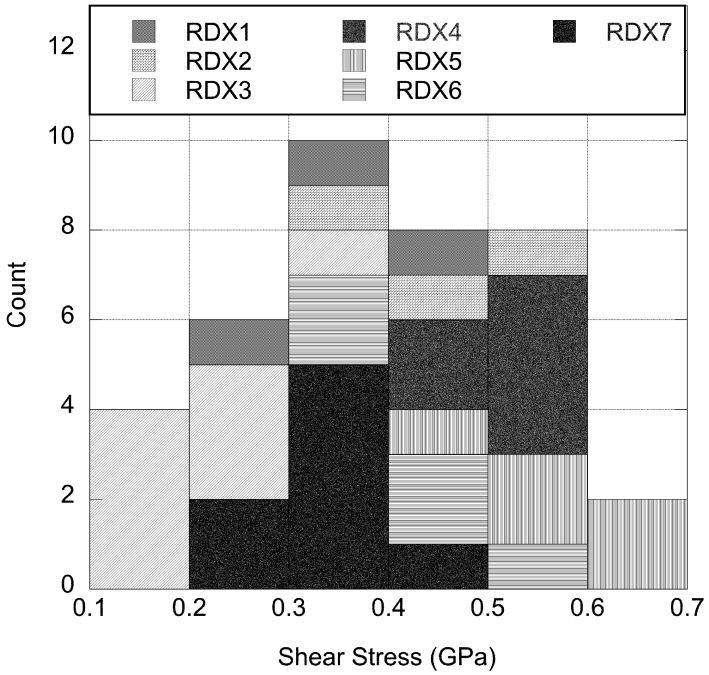

Figure 3.8. Histogram of shear stresses at which yielding occurs for each individual crystal. RDX crystals vary in strength, giving a broad distribution between 0.1 and 0.7GPa.

In the case of RDX, the sub-mm form of the material tested exhibits a distribution in the yield points that is indicative of mechanical or thermal cleaving of larger cm-scale single crystals, suggesting that powders of small RDX crystals include a substantial defect (likely dislocations) content on their surfaces.

3.6 Acknowledgments

We gratefully acknowledge the support of the US Air Force Office of Scientific Research under grant number FA9550-16-1-0101. Additionally, we would like to thank Dr. Steve Son, Purdue University for providing the raw materials in this study and for his input and thoughtful discussions.

4. CHAPTER: NANOINDENTATION OF ENERGETIC MATERIALS

In order to see if the dislocation activation demonstrated in the elastic-plastic transition in RDX is supportive of the dislocation pile-up mechanism for hot spot initiation a variety of energetic materials were selected for indentation to compare yield behavior. The materials used were cyclotetramethylene tetranitramine (HMX), 1,3,5-triamino-2,4,6-trinitrobenzene (TATB), 1,1-diamino-2,2-dinitroethylene (FOX-7), azodiaminoazoxyfurazan (ADAAF) and a trinitrotoluene and 2,4,6,8-hexanitro-2,4,6,8,10,12-hexaazatetracyclododecane cocrystal (TNT/CL-20). All materials were received from Los Alamos National Lab in our collaboration with them. While the explosive properties of these materials are well characterized, several have yet to have any mechanical characterizations published in the literature as they are either newer materials (ADAAF) or are very difficult to work with experimentally (TATB, TNT/CL-20). The information available, as far as could be found at present time, for the hardness and modulus of these are limited to values given by simulations. HMX and FOX-7, both similar to RDX in element composition ratios, are more well studied energetic materials that have had their hardness and modulus measured by several nanoindentation studies. Figure 4.1 gives the chemical structures of all listed materials, TNT and CL-20 are shown separately and not as a cocrystal formulation.

The experimental procedure for all materials was the same as that reported for aspirin and RDX in sections 2.1 and 3.3.2, indents were done using the load functions given in section 3.3.2 for both high-load and low-load indents. High load indents were used for similar analysis of each material regarding hardness, modulus, yield points (pop-ins), and shear stress. Low load and in some cases partial-unload indents were used to confirm that behavior prior to pop-ins was purely elastic. Elastic behavior is seen when the unload portion returns to the origin in the load-depth curve, meaning

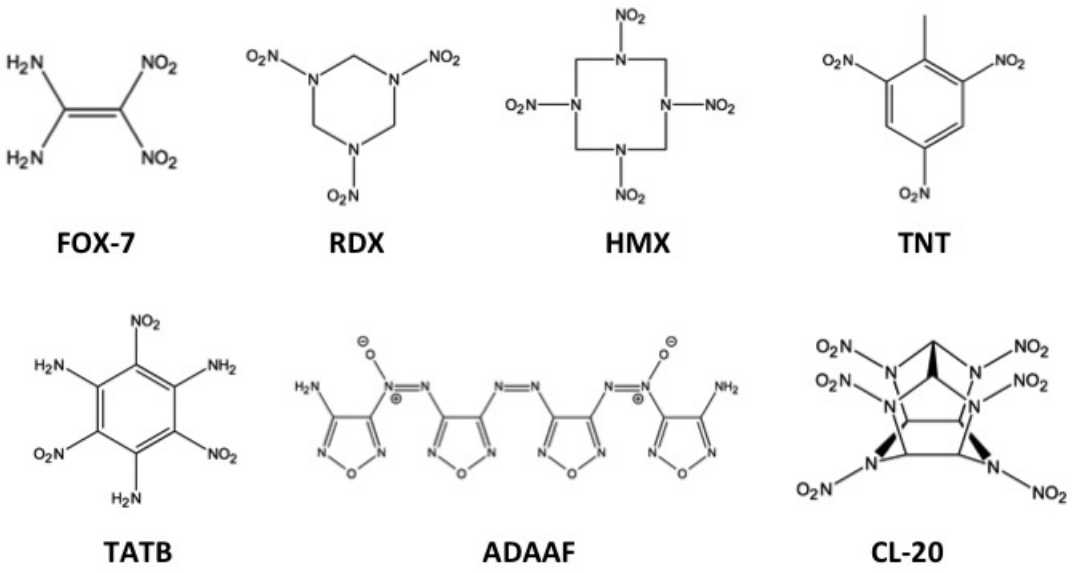

Figure 4.1. Chemical structures of selected energetic materials.

there was no indent left behind and therefore no plastic deformation. In Figure 4.2 an image of each type of crystal indented, except TATB, is given.

TATB had one procedural difference from the rest of the samples because the surface of the TATB was incredible rough. However, TATB has a very similar morphology to graphene, consisting of multiple layers. Scotch tape was used to remove the top layer by just touching the tape to the surface and removing it. This provided an incredibly smooth surface on the newly exposed layer, Figures 4.3(a) and 4.3(b) give before and after images of a TATB crystal.

Additionally the length of the yield point excursion and the energy release associate with the excursion were calculated. The energy released corresponds to the energy in transitioning from elastic deformation to plastic deformation. This can be found by taking the area under the loading curve to the end of the pop-in excursion and subtracting out the area corresponding to only plastic deformation, as illustrated in Figure 4.4.

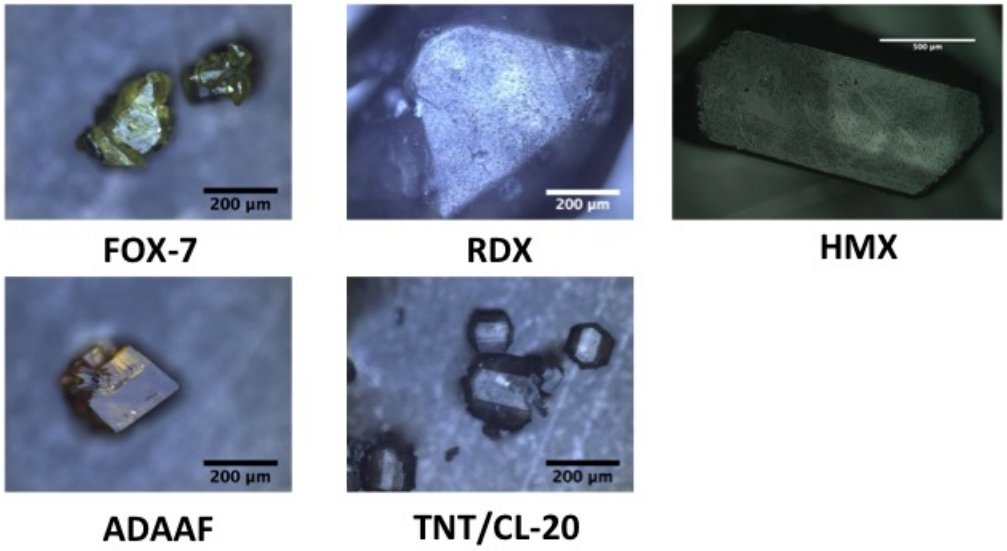

Figure 4.2. Images of example energetic crystals that were indented, scale bar is 200μm for all crystals except for HMX the scale bar is 500μm

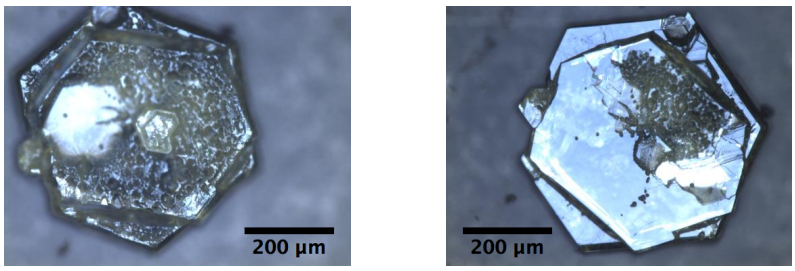

(a) Original TATB (b) TATB afterwards

Figure 4.3. Images of TATB crystals before and after removing a surface layer

The length of the excursion was looked at in addition to the area as it is less susceptible to errors associated with pseudo-elastic deformation. Even though indents were done in the elastic region to verify that deformation was elastic prior to pop-ins, there may have been indents were this was not the case. If there was plastic deformation prior to pop-in then the severity, or length of the excursion would decrease slightly, however the area under the curve would decrease much more dramatically

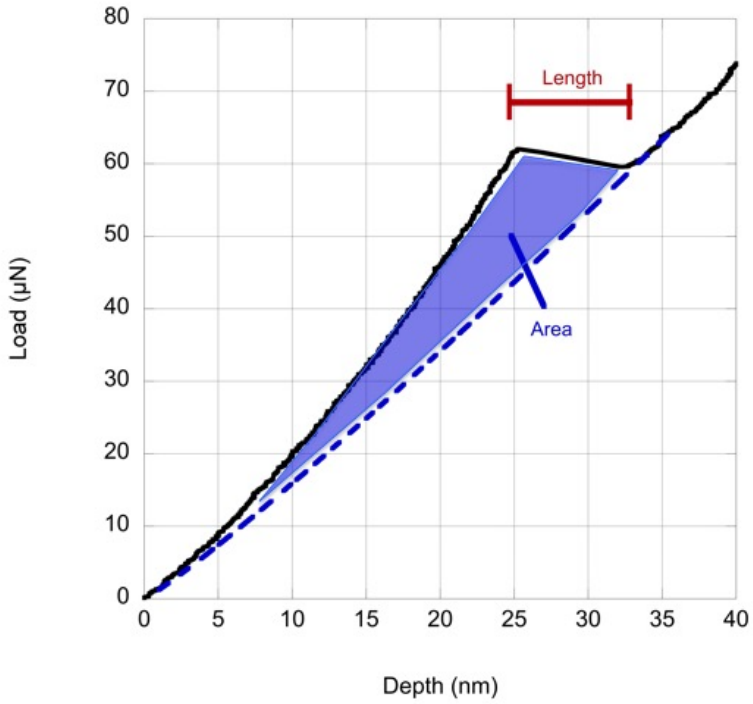

Figure 4.4. The length and area of excursions used.

with small changes in the displacement. By looking at both the energy and length of the excursions this potential source of error can hopefully be identified and minimized. In the following sections 4.1-4.5 the results for each material as well as comparisons to literature values, if available, are presented. Section 4.6 then summarizes these and notes trends seen between the current work and drop weight sensitivities.

4.1 HMX

There are four reported polymorphs of HMX, however β-HMX ($C_4H_8N_8O_8$ monoclinic, $P2_1/n$ space group) is the stable form at room temperature [53]. HMX is one of the easier energetic materials to grow as large single crystals, and there have been several nanoindentation studies of HMX with crystals that were grown to millimeter [54] and even centimeter scales [55]. This allows for a direct comparison on the

properties of specific faces on large single crystals to the averaged properties given in this study of multiple crystals.

The cited studies on millimeter and centimeter sized HMX by Kucheyev et al. and Li et al. both used evaporative methods to crystallize HMX from an acetone solution. Kucheyev et al. used both Berkovich and spherical diamond tips to indent the (010) surface of their samples with loads of 50 and 100mN depending on the tip. Results from indentations done with the Berkovich tip give a modulus of 17.6GPa and a hardness of approximately 0.7GPa. Cracking was observed primarily in the [100] in residual indent impressions after indents done both by Berkovich and spherical tips. Li et al. used a Berkovich tip to indent the (010) and another random non-indexed face for comparison, using 600μN as the maximum indent load. They also perform indents using up to 4mN loads to compare values measured at different depths. The average reported modulus and hardness for the (010) face was 23.18 and 1.13GPa respectively. The modulus of the second random face indented was 26.05GPa and the hardness 0.95GPa. Kucheyev comments that the values they obtained were much lower than the values reported by Li's group, however they do not offer an explanation as to why. One potential reason for this as they mentioned in their own paper is the presence of cracks in the residual indent impressions. Li's group used much lower loads of 600μN, compared to Kucheyev's 50mN, nearly an order of magnitude lower, and while they suspected cracking to occur and claim this is the case, do not show any data supporting this. Pop-ins in the load-depth curve are not necessary indicative of cracks in the sample, as has been shown to be the case in chapter 3 with RDX. 600μN may not a sufficient load to induce cracking in HMX as loads of 1000μN were used in this study and no cracking was observed. However at much higher loads, such as 50mN, it stands to reason cracks will form in the samples. This can cause a decrease in the measured properties as perceived contact area will be larger. It is believed for this reason that the results presented here match more closely those measure by Li's group.

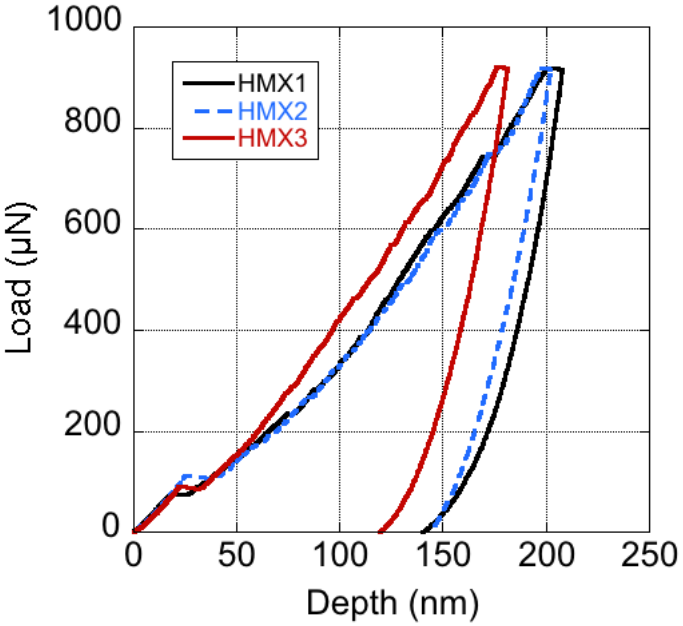

(a) Representative load depth curves

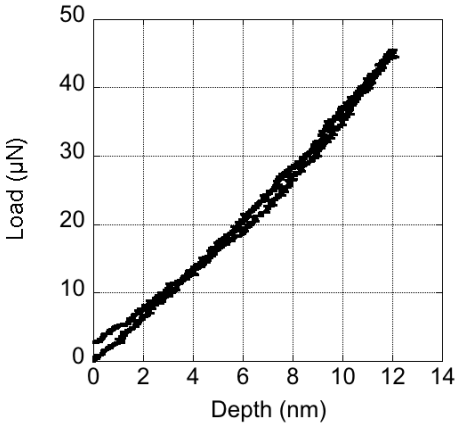

(b) Low-load indent showing elastic deformation

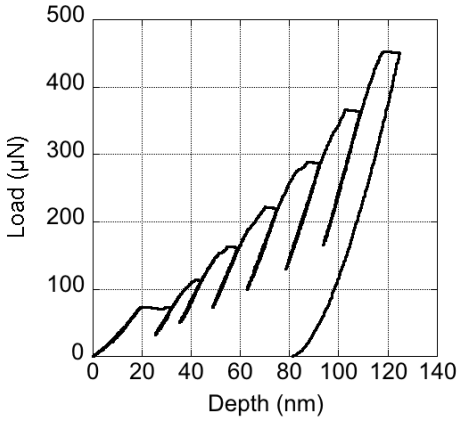

(c) Partial-unload indent with seven steps

Figure 4.5. Selected load depth curves for HMX

Three HMX crystals were mounted for indentation, the faces tested were not indexed. Each sample was indented ten times, a load-depth curve from each crystal is given in Figure 4.5, along with a low-load and a partial unload indent. The hardness and modulus of each HMX crystal and given in Figure 4.6.

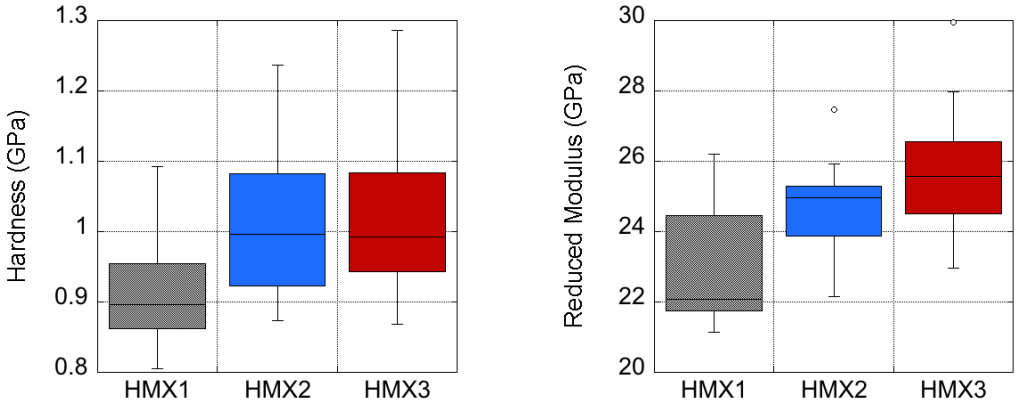

(a) Hardness of HMX crystals

(b) Modulus of HMX crystals

Figure 4.6. Box and whisker plots showing the mean, median, upper and lower quartiles for the properties of HMX crystals obtained from final unloading segments.

The average hardness and modulus over all crystals indent was 24.5±1.3 and 0.99±0.06GPa respectively. As mentioned these values are in good agreement with those reported by Li's group in 2010. HMX1 gives the lowest values for both hardness and modulus, while HMX2 and HMX3 gave near identical results. This could mean that HMX2 and HMX3 had the same crystallographic face tested while HMX1 was a different face. A residual indent image is given in Figure 4.7 that shows no evidence of any surface cracks at these loads. Other images of residual indents similarly do not show any signs of cracking.

A majority of indents demonstrated pop-in behavior, however several indents showed no sign of pop-ins, instead plastically deforming from the start of the indent. These points were excluded from the yield behavior analysis as they do not conform to the Hertzian contact model assumptions of being elastic. Figure 4.8 demonstrates indents that contain pop-ins and those that do not. While these points were excluded it does not mean they were overlooked, it simply means that the current model used is not adequate for application in all scenarios and other additional methods may need to be looked at for indents exhibiting only plastic deformation. This becomes

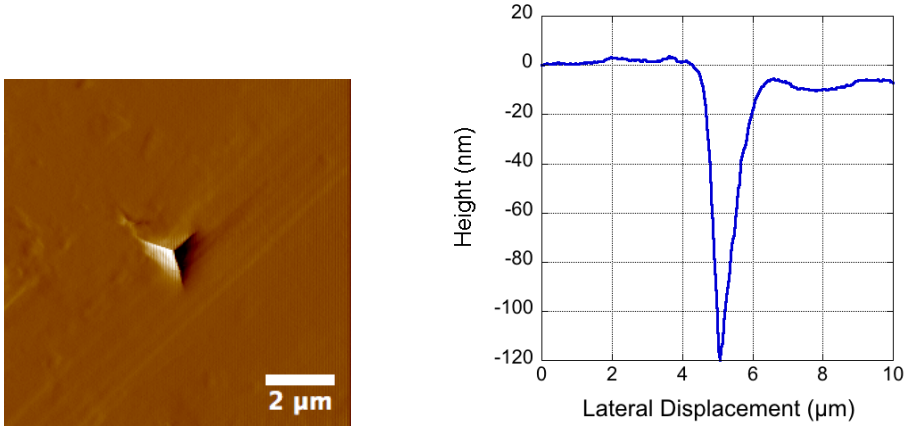

(a) Residual indent impression

(b) Height profile bisecting indent from corner to edge

Figure 4.7. Residual indent impression and height profile on HMX demonstrates that there are no surface cracks present

more relevant in softer materials where plastic deformation is dominant over elastic deformation even at low loads.

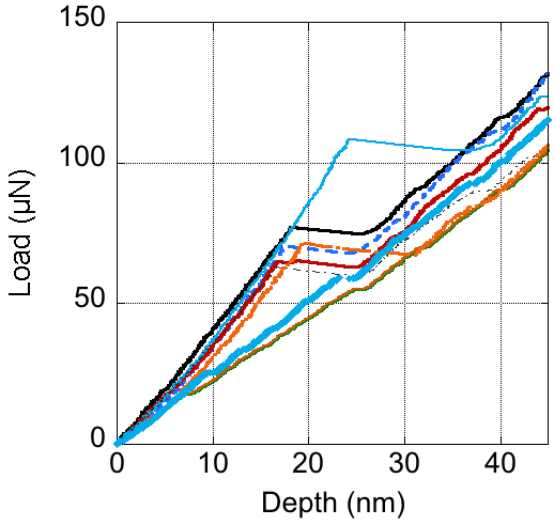

Figure 4.8. Examples of pop-ins and plastic deformation observed in HMX load depth curves

From the pop-in behavior the load at which these yield points occurred is given in Figure 4.9, from which the shear stresses at which HMX yielded were calculated using equation (1.4) and are given in Figure 4.10. The shear stresses are shown for each individual crystal and indicate that in general HMX3 was the strongest while HMX1 was the weakest, and HMX2 was somewhere in-between. The cumulative fraction plot, Figure 4.9(b), has a long extended tail at higher loads, very similar to the behavior seen in RDX. The average length of excursions was found to be 9.5±4.5nm and the average energy of the excursions was 556±290μN*nm. The standard deviation of these values is quite large, possibly because the nature of the excursion is dependent on the local dislocation density which can vary greatly from point to point.

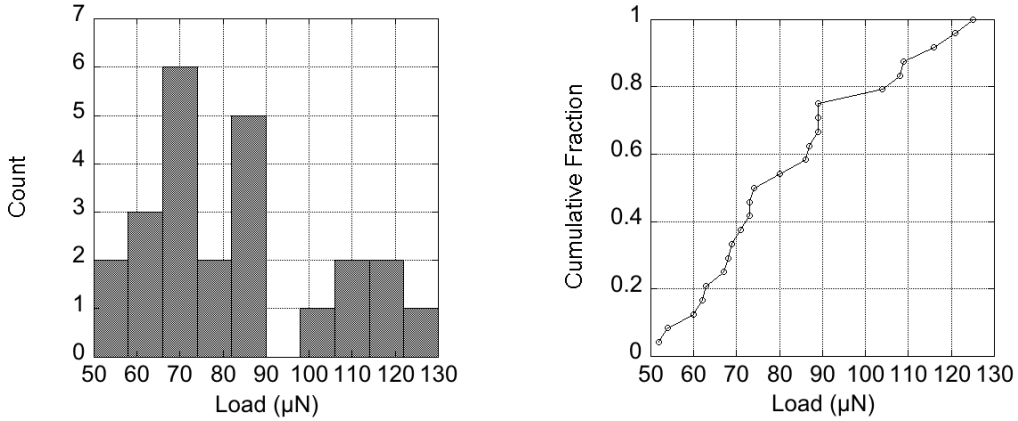

(a) Histogram of yield point loads

(b) Cumulative fraction of yield point loads

Figure 4.9. Histogram and cumulative fraction of the loads at which the initial yield phenomena occurred as a pop-in

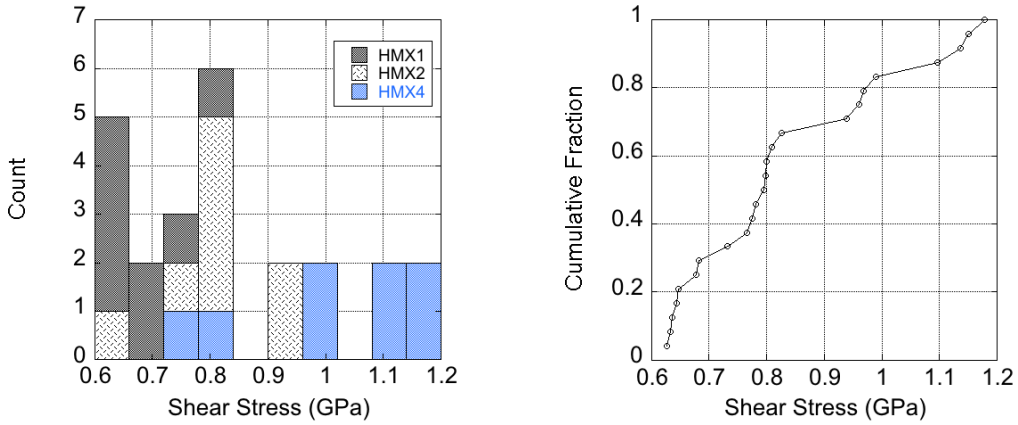

(a) Histogram of yield point shear stresses

(b) Cumulative fraction of yield point shear stresses

Figure 4.10. Histogram and cumulative fraction of the shear stresses at which the initial yield phenomena occurred as a pop-in

4.2 TATB

TATB ($C_6H_6N_6O_6$ triclinic, $P\bar{1}$ space group [56]) is a very powerful but insensitive secondary explosive. It has a graphite-like morphology that allows it to slip easily in specific planes. Molecular dynamics simulations of the nanoindentation of TATB were done by Mathew et al. in 2016, but there has been no experimental evidence to verify their calculations [57]. They simulated indentations on the (001), (010), and (001) planes of TATB using a spherical indenter at 77K. Their reported moduli for those respective faces are 27.7, 26.0, and 10.7GPa. The simulation results show the highly anisotropic nature of TATB, having nearly a factor of two difference on the modulus between different faces. The hardness is reported as 1.02GPa for the (001) face, but could not be computed for the other faces for computational reasons due to the depth of the indentation on these planes.

The hexagonal, plate-like nature of the TATB made it rather difficult to mount. Additionally, using scotch tape to remove the top layer often resulting in pulling the entire specimen off of the steel disk mount if the procedure was not done carefully. Being able to test the sides of the plate-like TATB at this point could not be achieved.

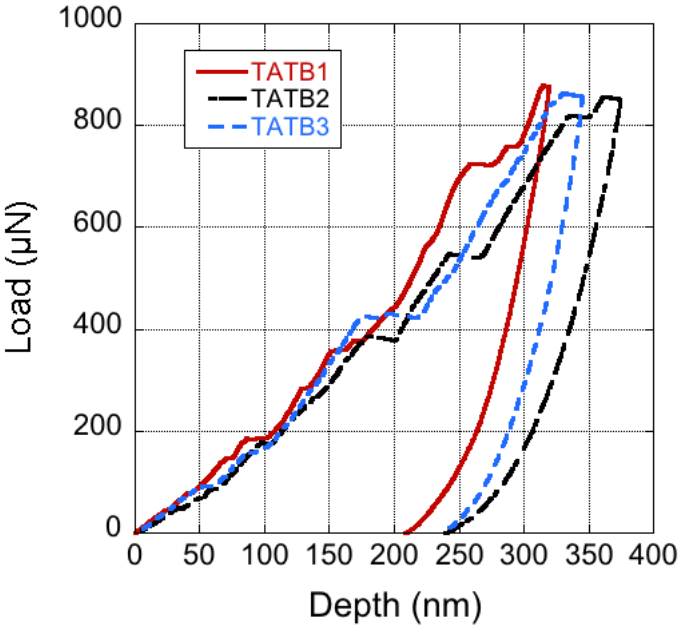

(a) Representative load depth curves

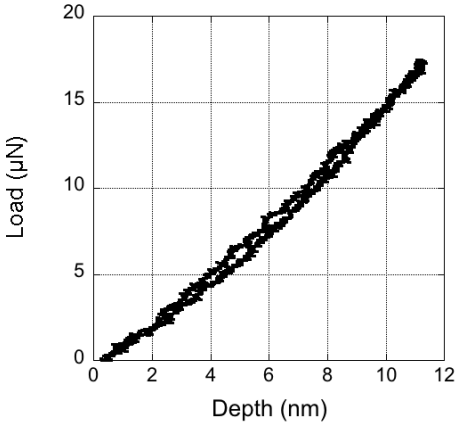

(b) Low-load indent showing elastic deformation

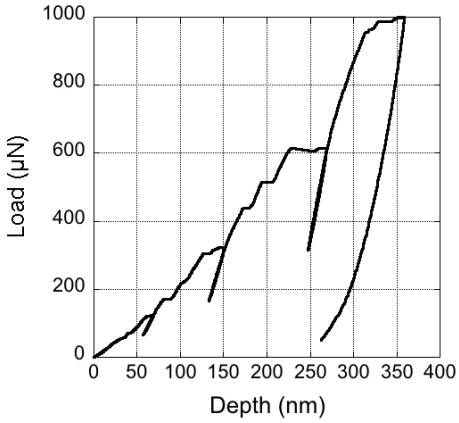

(c) Partial-unload indent with five steps

Figure 4.11. Selected load depth curves for TATB

A total of three good crystals with smooth surfaces were prepared and an average of five indents was done per crystal. Load-depth curves for each crystal are shown in Figure 4.11. The hardness and modulus are given in Figure 4.12. The hardness of the crystals is rather uniform, however there is some variations present the modulus with

TATB2 seemingly having a much lower modulus. The modulus of TATB2 also has an outlier point in Figure 4.12(b) that is near the values of TATB1 and TATB3. this could be a genuine outlier or it could indicate that this crystal had some other factor that decreased the modulus, perhaps by using tape on the surface, giving it a lower value than the actual value in the areas indented and this outlier point was one that remained unchanged. The average hardness and modulus over all three crystals was 0.41±0.04 and 9.6±1.5GPa respectively, which is very similar to the reported simulation modulus of 10.7GPa for the (001) face. This is very close agreement considering the conditions used for the simulation at liquid nitrogen temperatures and using a spherical tip do not reflect the actual experimental conditions. Molecular dynamics also have a tendency to over estimate nano-indentation values as tip conditions in reality are not ideal compared to the geometry boundaries used in simulations.

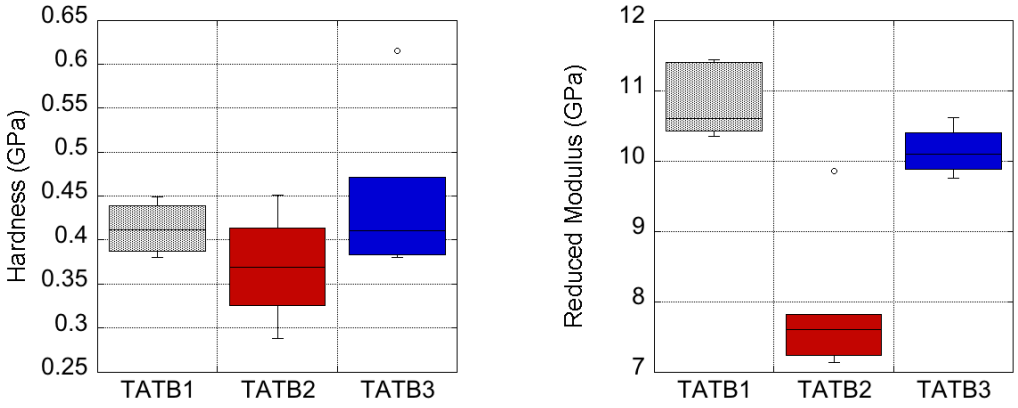

(a) Hardness of TATB crystals

(b) Modulus of TATB crystals

Figure 4.12. Box and whisker plots for the properties of TATB crystals obtained from final unloading segments.

Figure 4.13 gives an image of an indent, these indents also show no signs of cracking at the applied loads in TATB. There is significantly more pile-up present than in HMX or RDX. As can be seen in Figure 4.11(b) TATB behaves elastically at low loads, however the yield behavior is much less distinct. There tends to be a very clear elastic portion followed by just a change in slope, or "wobbles" in the load

depth curve rather than distinct pop-ins, though in some cases clear excursions are visible. The behavior at low loads is shown in Figure 4.14.

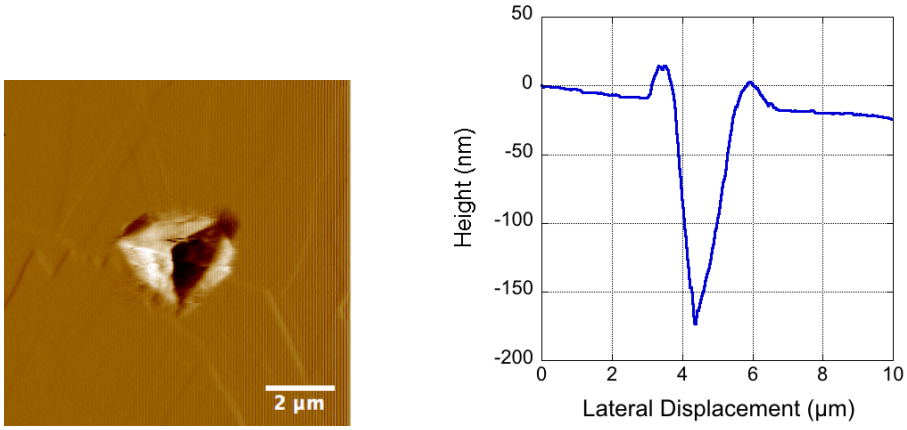

(a) Residual indent impression

(b) Height profile bisecting indent from corner to edge

Figure 4.13. Residual indent impression and height profile on TATB shows no signs of cracking, but has significant pile-up

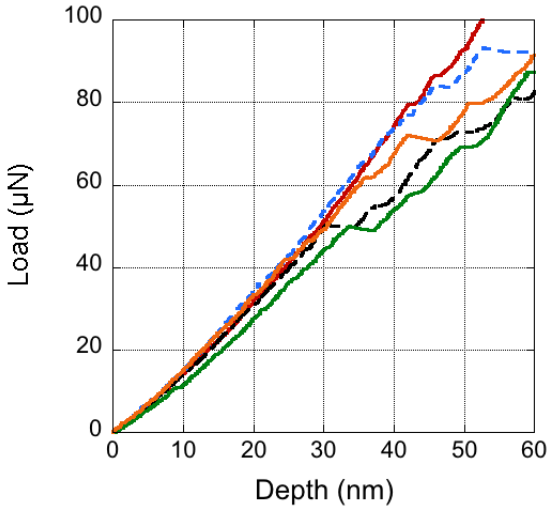

Figure 4.14. Examples of pop-ins and plastic deformation observed in TATB load depth curves

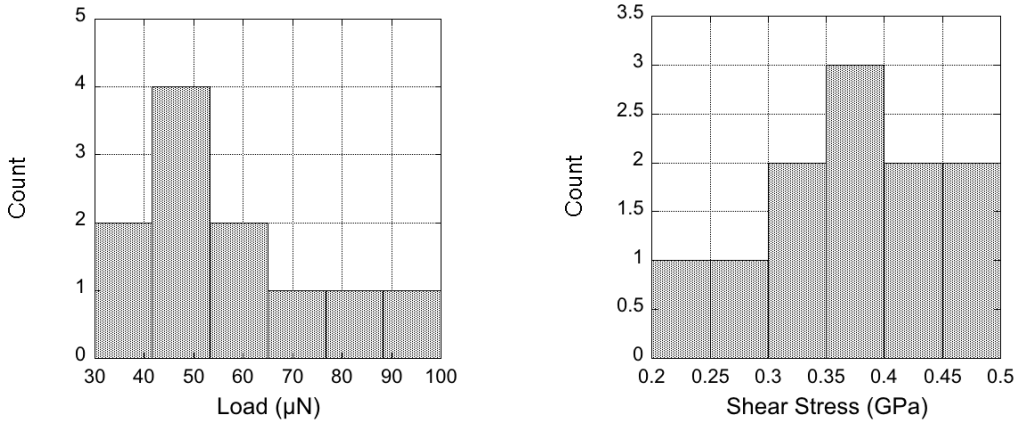

(a) Histogram of yield point loads

(b) Histogram of yield point shear stresses

Figure 4.15. Histograms of the load and shear stresses at which the initial yield phenomena occurred in TATB

The loads and shear stresses were still calculated for TATB, it was just taken at the point where there was a deviation in the slope of the load depth curve (deviation form the Hertzian model) in cases where excursions were not visible. These are given in Figure 4.15, cumulative fractions were not included as the number of indents done was significantly less histograms were considered sufficient. The average length and energy of the yield point excursions were 2.8±2.2nm and 98±95μN*nm. Again there are large variations in these values, particularly as TATB does not always exhibit horizontal pop-ins and often the onset of plastic deformation is seen as a deviation in the slope of the curve. The difference in behavior of TATB at yield could be a result of different dislocation behavior on the surface, and may be one factor in its insensitive behavior.

4.3 FOX-7

FOX-7 ($C_2H_4N_4O_4$ monoclinic, $P2_1/n$ space group [58]), with the same chemical composition ratio as RDX and HMX, is a material of interest as it is less sensitive than either RDX or HMX but has similar energy density. FOX-7 is another material

that is difficult to grow as large crystals, however Zhou et al. performed nanoindentation experiments on FOX-7 crystals that had been grown by adding a morphological modifier [31]. Their study, while useful as the first of its kind done on FOX-7, suffers from several of the pitfalls mentioned in section 1.3 on sample preparation. They grow incredibly large crystals with the addition of a crystal growth agent, which may change the mechanical properties and does not necessarily provide an accurate representation of the properties of FOX-7 actually used in applications. They also subject the surface of their samples to multiple smoothing process that can alter measured surface properties: cutting the faces with a diamond wire saw, polishing with alundum, and polishing with cerium oxide. Despite these their study provides a good comparison as no one else has managed to experimentally use nanoindentation to study FOX-7. Zhou's group uses a Berkovich tip and indents the (020), ($\bar{1}$01), and (002) faces with loads of 8mN. The modulus for all three faces was 11.09, 16.65, and 21.34GPa respectively and the hardness values were 0.52, 0.63, and 0.67GPa. They also note that they observe pop-ins in indentations on each face that they call signs of "intermittent plastic flow", and describe the depth and loads at which some of these occur.

FOX-7 crystals were mounted and six samples were selected for indentation, an average of 6 indents was performed on each crystal. Sample load depth curves for each crystal are presented in Figures 4.16.

The behavior of FOX-7 is slightly different than that of previously measured materials as there is an increased amount of plastic deformation early in the loading portion of the indent. This can be seen in Figure 4.16(b) where the unload segment does not return to the original and about a 1nm deep impression is left behind. Several FOX-7 indents had elastic behavior, however a majority showed plastic deformation from the start. Several loading portions of indents are given in Figure 4.17 that demonstrate some behavior like TATB with kinks in the plot and some that demonstrate behavior like HMX with evident pop-ins.

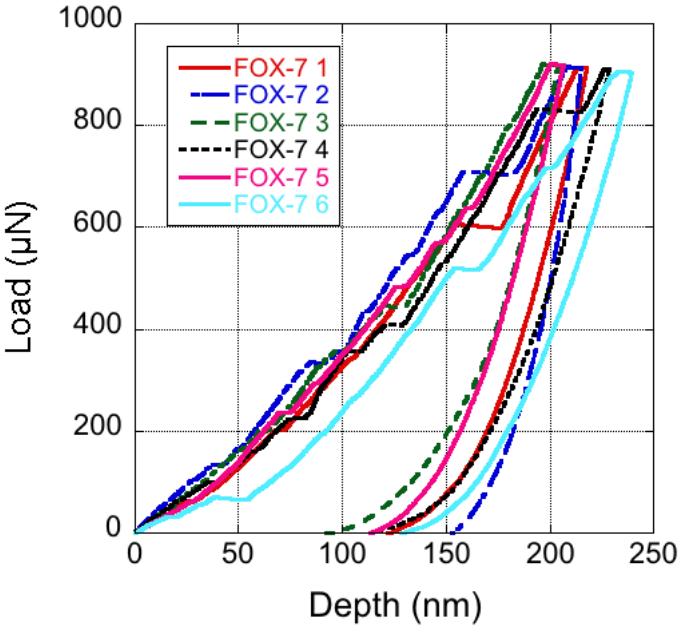

(a) Representative load depth curves

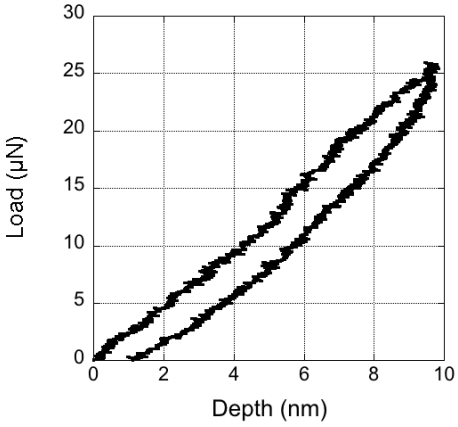

(b) Low-load indent showing some plastic deformation

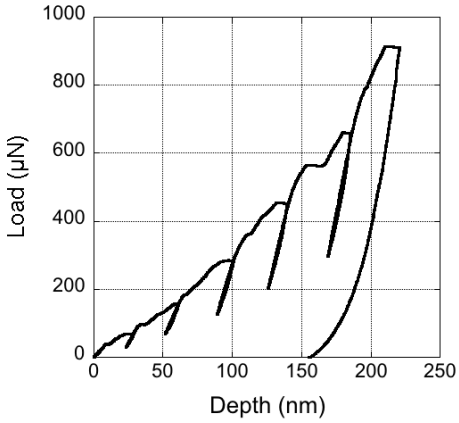

(c) Partial-unload indent with seven steps

Figure 4.16. Selected load depth curves for FOX-7

An image of an indent is given in Figure 4.18. The surface has some roughness and pits evident around the indent on the edges of the image. In general the surface of the FOX-7 samples was much poorer than those of the other samples tested. This is perhaps a justification of Zhou et al. polishing their sample surfaces as this is

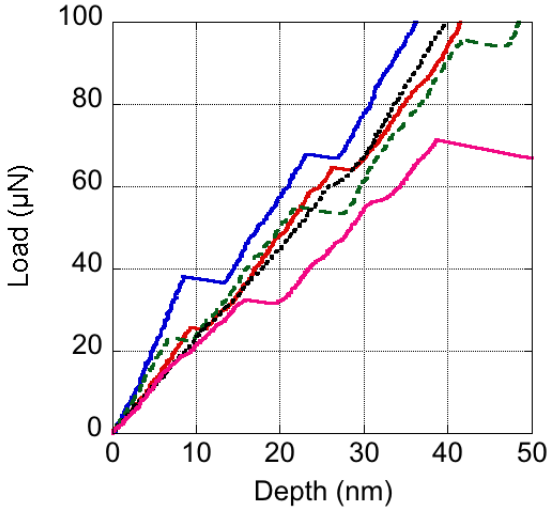

Figure 4.17. Several examples of plastic deformation observed in FOX-7 load depth curves with two examples of elastic behavior

the current limitation of the sample preparation. The average hardness and modulus for FOX-7 are 0.86±0.08 and 19.6±4.0GPa, Figure 4.19 gives the properties for each individual crystal. There is a small spread in the mechanical properties but that is to be expected when testing randomly orient faces of an anisotropic material. Most values of the modulus fall into the range reported by Zhou's group with the exception of FOX-7 2, which had a significantly higher modulus. The hardness values were also slightly higher, which may be due to the fact that no morphological modifier was added to these samples so that they retain their original hardness.

The plastic behavior of FOX-7 made it difficult to identify the first pop-in phenomena in all but a few cases. There were a total of four indents that showed clear plastic behavior with a distinct yield point. The loads at which these occurred were at 20, 22, 31, and 35μN, the shear stress at which these points occurred was approximately 0.2GPa, further analysis was not done as it seemed a bad application of the Hertzian model where the assumptions were not necessarily true. From these four indents the average length and energy of excursion was 4±0.7nm and 57±10μN*nm.

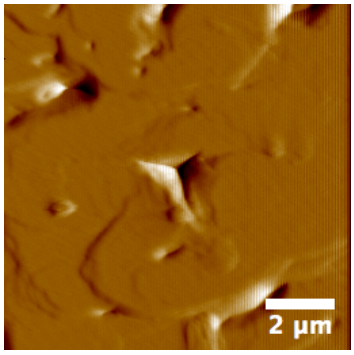

(a) Residual indent impression

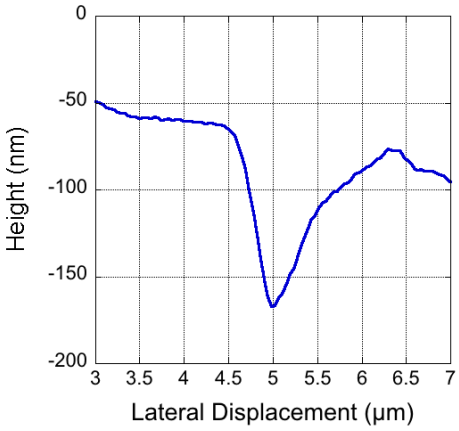

(b) Height profile bisecting indent from corner to edge

Figure 4.18. Residual indent impression and height profile on FOX-7

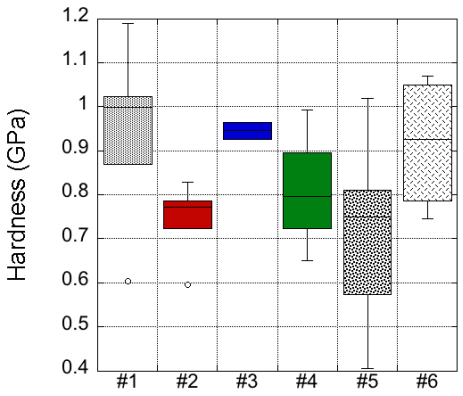

(a) Hardness of FOX-7 crystals

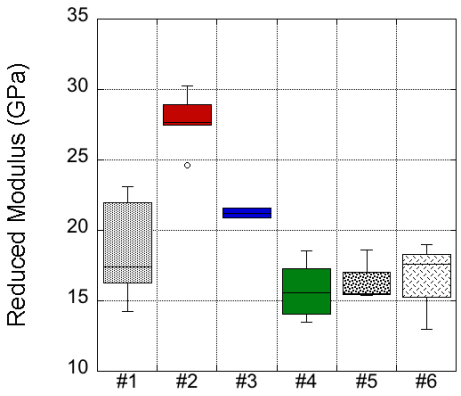

(b) Modulus of FOX-7 crystals

Figure 4.19. Box and whisker plots showing the mean, median, upper and lower quartiles for the properties of FOX-7 crystals obtained from final unloading segments.

These values are included in the analysis done in section 4.6 however it is noted that this particular information is an average based only on four data points.

4.4 ADAAF

ADAAF ($C_8H_4N_{16}O_6$ monoclinic, $P2_1/n$ space group [59]) is a more recent energetic material that has yet to have much literature published on it. The first paper that focuses on the synthesis and characterization of ADAAF was published in 2010 by Veauthier et al. from Los Alamos National Lab [59]. Since then there have been studies have focused on the heat of formation of furazans including ADAAF using density functional theory [60]. There has yet to be any nanoindentation studies or simulations done for ADAAF.

An average of five indents were performed on 8 ADAAF crystals. The behavior of these crystals was unlike any other energetic materials tested so far, in Figure 4.20(a) indents from only the first four crystals are shown, however the four crystals behaved in similar manners. It can be seen that all indents were completely smooth with non pop-in events. In Figure 4.20(b) it can be seen that there is a large amount of plastic deformation as soon as the indentation takes place. An image of an indent is given in Figure 4.21.

Most likely there are large amounts of plastic deformation causing the slope to be smooth rather than intermittent plastic deformation causing pop-in behavior. This is supported by the fact that ADAAF is an incredibly soft material with an average hardness and modulus of 0.23±0.09 and 6.7±1.3Gpa respectively, about a third the hardness of other materials tested. The hardness and modulus of each crystal is given in Figures 4.22 and 4.23. This behavior was quite curious and unexpected as it plastically deforms in all stages of the indentation, meaning there is significant dislocation density present in the material beforehand. This could be a result of the synthesis and handling, or it could be the nature of ADAAF as a very soft material. It would appear from the crystal image providing in Figure 4.2 that ADAAF is brittle as there seem to be edges and a corner where the crystal has broken off. Further studies would need to be done to determine the fracture behavior and brittleness of

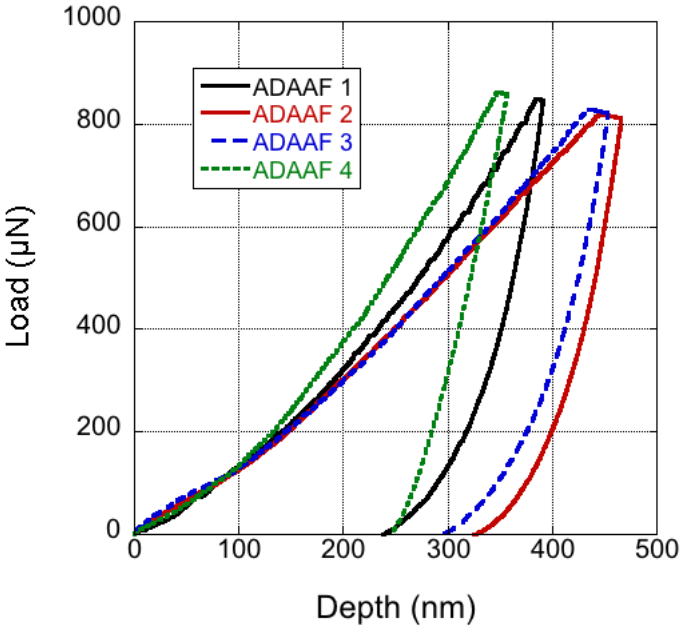

(a) Representative load depth curves

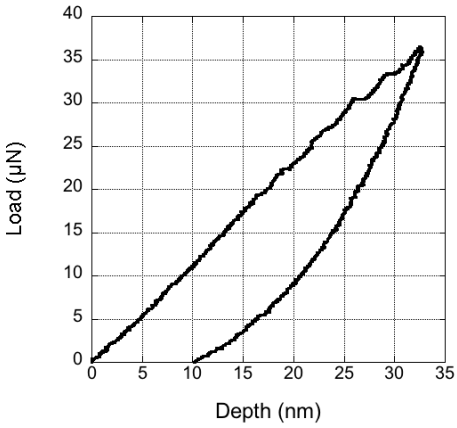

(b) Low-load indent showing some plastic deformation

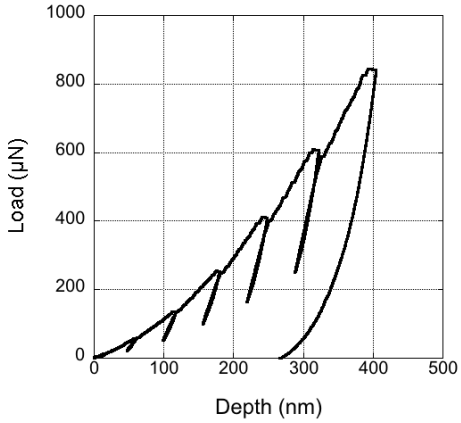

(c) Partial-unload indent with seven steps

Figure 4.20. Selected load depth curves for ADAAF

ADAAF and see if the large amount of plastic deformation at a small scale affects the bulk behavior.

The plastic behavior of ADAAF means that it falls outside of the assumptions made by the Hertzian model and cannot be interpreted in the same manner as the

previous materials have been. There is no analogous, simple contact model for plastic behavior suitable for application to indentation mechanics. This limits the measurement of mechanical properties to the hardness and modulus of ADAAF.

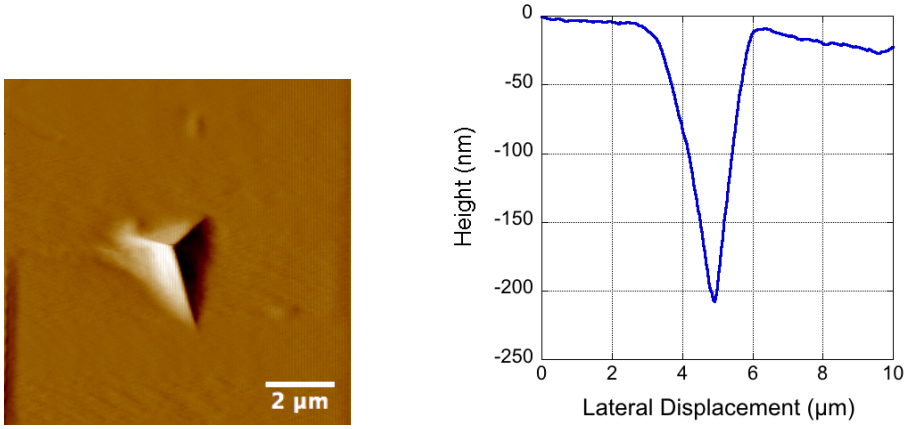

(a) Residual indent impression

(b) Height profile bisecting indent from corner to edge

Figure 4.21. Residual indent impression and height profile on ADAAF

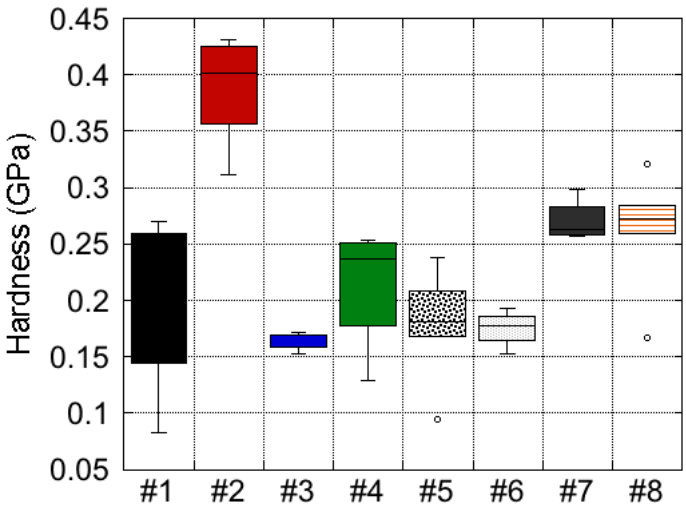

Figure 4.22. Box and whisker plots showing the mean, median, upper and lower quartiles for the hardness of ADAAF crystals obtained from final unloading segments.

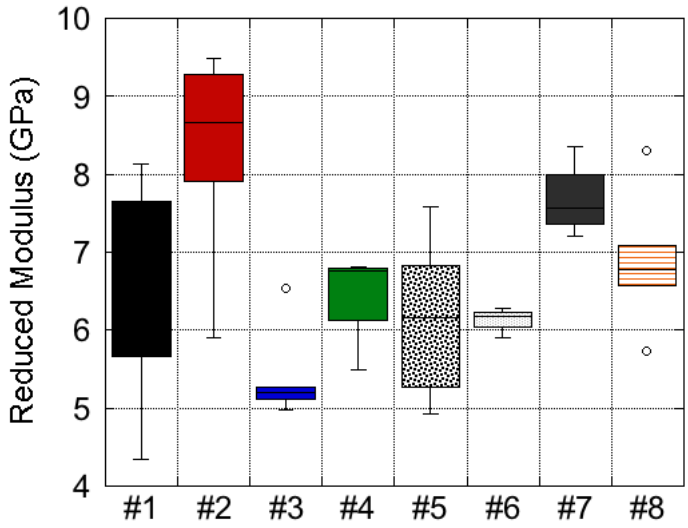

Figure 4.23. Box and whisker plots showing the mean, median, upper and lower quartiles for the modulus of ADAAF crystals obtained from final unloading segments.

4.5 TNT/CL-20 Cocrystal

Cocrystals are of great interest in both the pharmaceutical and energetics community. By combining two compounds into a single crystal structure the hope is to be able to modify the resulting properties to better suit the needs of the application. For pharmaceuticals this is done with hopes of improving solubility, drug delivery dosage, and other properties relating to the active pharmaceutical ingredients [61, 62]. In energetic materials the desire is to use cocrystals to develop more stable explosives with higher energy [63, 64]. Many cocrystal formulations exist and nanoindentation has been one method used in determining their mechanical properties, particularly in pharmaceuticals [65, 66]. Nanoindentation of energetic cocrystals has received much less attention, partly due to the difficulties in growing suitable samples for indentation.

TNT/CL-20 (orthohombic, Pbca space group [63]) is an energetic cocrystal of interest as it seems to maintain some of the high energy density of CL-20 but is less

sensitive than CL-20. While forming cocrystals does not necessitate that the resulting properties should be an average of the properties of the pure components, it has been shown for TNT/CL-20 that this seems to be the case [64, 67]. Molecular dynamics simulations of TNT/CL-20 predict a Young's Modulus of 17.891GPa [68], though this is slightly different from the reduced modulus obtained from nanoindentation it is a comparable value. The relationship between the Young's modulus, E, and the reduced modulus, E_r, is given by

$$\frac{1}{E_r} = \frac{1-\nu_i^2}{E_i} + \frac{1-\nu_s^2}{E_s}, \tag{4.1}$$

where the s and i subscripts refer to the sample and the indenter.

The average reduced modulus, determined from a total of eleven indents done on three different cocrystals, was measured to be 14.2±1.2GPa. The average hardness was measured to be 0.63±0.13Gpa. The closeness in the values of 14.2GPa for a reduced modulus and 17.891GPa for a predicted Young's modulus is encouraging as both numbers are in the same ballpark values. While the experimental values reflect the reality of the material, it verifies that methods used for simulating new materials such as cocrystals are sufficient for first approximations. Hardness and modulus values are not shown for each sample as two smaller crystals only had 2 indents done on them while the third larger crystal had 7 indents done on it. On crystals only tens of microns in size multiple indents cannot be done without sufficient spacing between them to prevent overlapping their plastic zones in the crystal.

An image of the residual impression left by the indenter is given in Figure 4.24. It can be seen that there is very little pile-up surrounding the indent, similar to the harder energetic materials, even though the cocrystal is a much softer material. Load depth curves of indents done on each crystal are given in Figure 4.25(a). Also shown in Figure 4.25(b) and 4.25(c) are a low load indent demonstrating plastic behavior and a zoomed in view of the initial loading behavior. It can clearly be seen that the TNT/CL-20 cocrystal behave elastically until the first yield point pop-in. No partial-unload indents were performed on the TNT/CL-20 sample as there were not enough samples and not enough surface area to do additional indents other than those needed

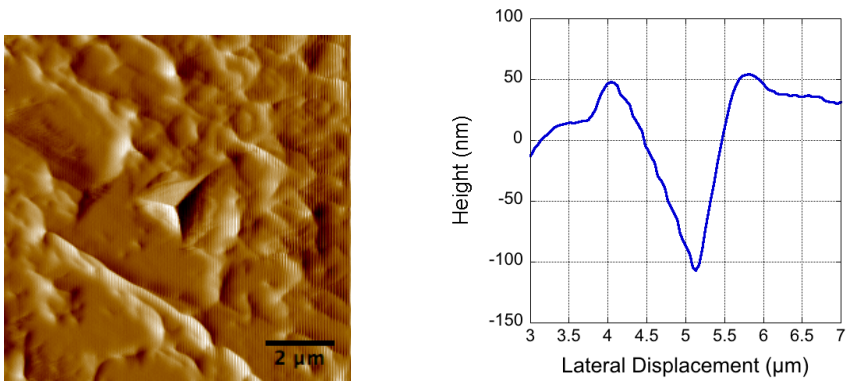

(a) Residual indent impression

(b) Height profile bisecting indent from corner to edge

Figure 4.24. Residual indent impression and height profile on TNT/CL-20

for measurements done on the hardness and modulus. The average excursion length and energy were 5.9±3.7nm and 238±151μN*nm.

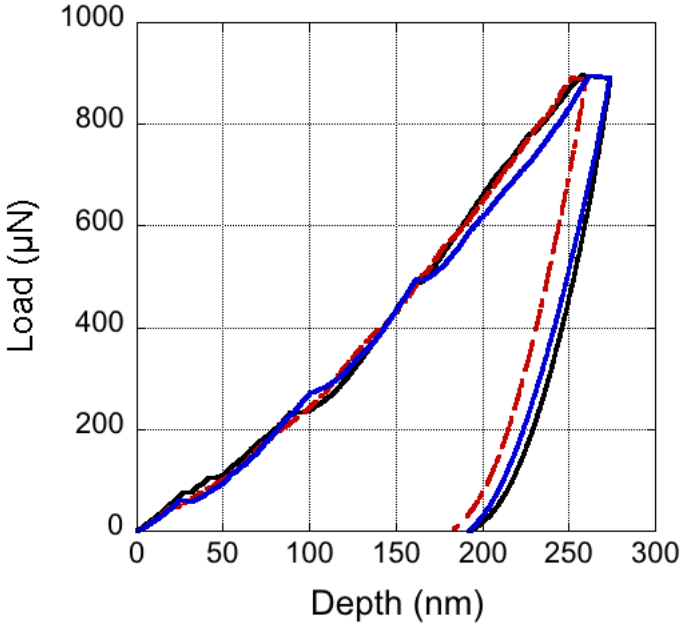

(a) Representative load depth curves

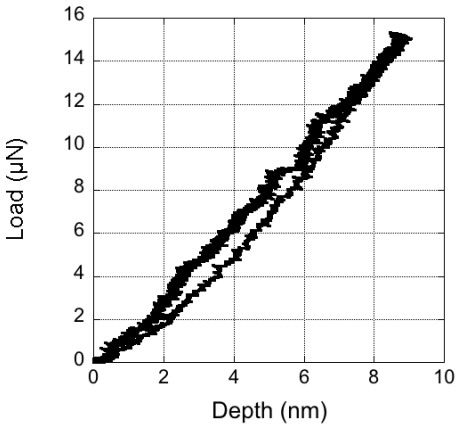

(b) Low-load indent showing elastic behavior

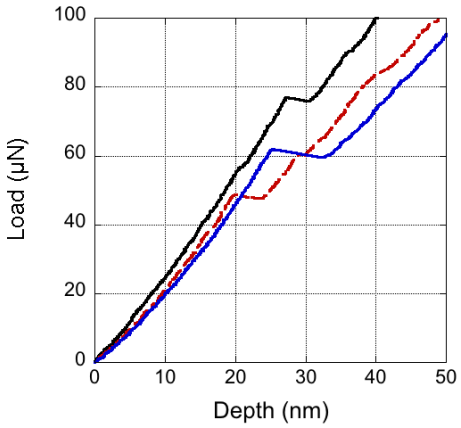

(c) Loading portion showing initial pop-in

Figure 4.25. Selected load depth curves for TNT/CL-20 cocrystal

4.6 Trends and Drop Weight Sensitivity

The mechanical properties of six different energetic materials were measured through nanoindentation. A summary of the hardness and modulus of each material is give in Table 4.1. Also given in Table 4.2 is the shear stress values at yield for each material.

Table 4.1.
Mechanical Properties of Energetic Materials

Material	E_r **(GPa)**	H **(GPa)**	# of Crystals	Total # Indents
TATB	9.6 ± 1.5	0.41 ± 0.04	3	14
FOX-7	19.6 ± 4.0	0.86 ± 0.08	6	23
RDX	19.1 ± 3.0	0.74 ± 0.10	6	33
HMX	24.5 ± 1.3	0.99 ± 0.06	3	30
ADAAF	6.7 ± 1.3	0.23 ± 0.09	8	41
TNT/CL-20	14.2 ± 1.2	0.63 ± 0.13	3	11

Table 4.2.
Shear Stress at Yield in Energetic Materials

Material	τ_{min} (GPa)	τ_{max} (GPa)	τ_{avg} (GPa)	τ_{avg}/E_r
TATB	0.24	0.48	0.38	0.040
FOX-7	0.24	0.48	0.38	0.019
RDX	0.13	0.65	0.39	0.020
HMX	0.63	1.18	0.83	0.034
ADAAF*	-	-	NA	NA
TNT/CL-20*	-	-	NA	NA

*no yield behavior or not enough data

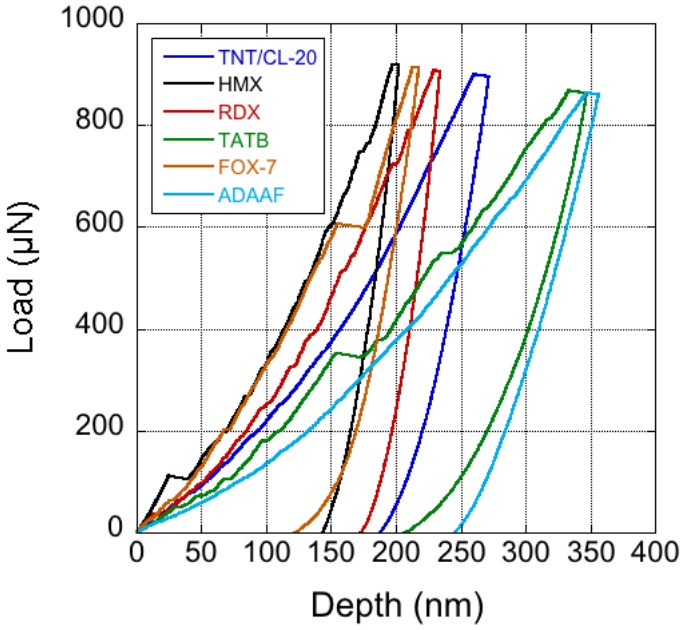

Figure 4.26. One load depth curve of each material

Nanoindentation is a valuable tool for measuring these properties, particularly for ADAAF, TATB, and TNT/CL-20, for which these properties have never been measured experimentally before. A load depth curve from each material is shown on the same plot in Figure 4.26 for comparison. For each material the drop weight sensitivity determined by the drop height, H_{50}, was obtained from Los Alamos National Lab (LANL). Figure 4.27 shows a plot of the energy of excursions verse H_{50}. ADAAF, which did not have any pop-ins, is not included in this figure but has an H_{50} of 34.2cm as reported by LANL.

It can be seen that in general the more sensitive materials have more energetic pop-ins. This also becomes more apparent when looking at the length of pop-ins, given in Figure 4.28. The length verse drop height shows the same trend as the energy plots but the placement of FOX-7 falls more in line with the other materials. This is probably because of the mentioned pseudo-elastic deformation causing the energy of excursion to be lowered while the length of excursion is not greatly affected. FOX-7 being more prone to plastic deformation sees this large decrease in the excursion

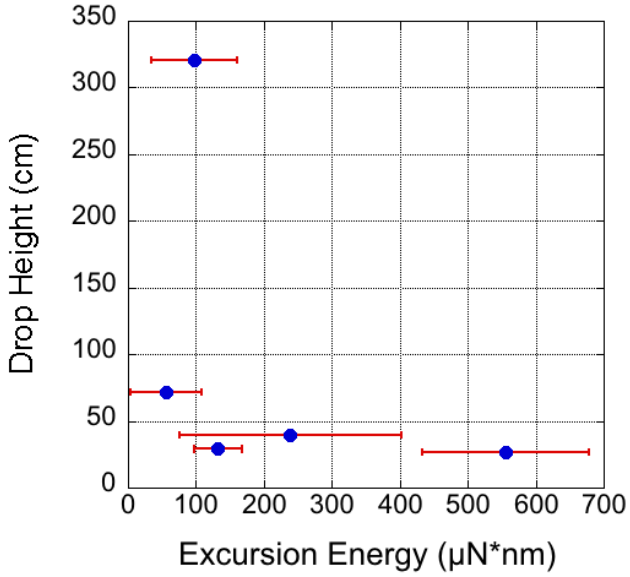

Figure 4.27. Average excursion energy of each material verse H_{50}, errors bars are given by the 95% confidence interval.

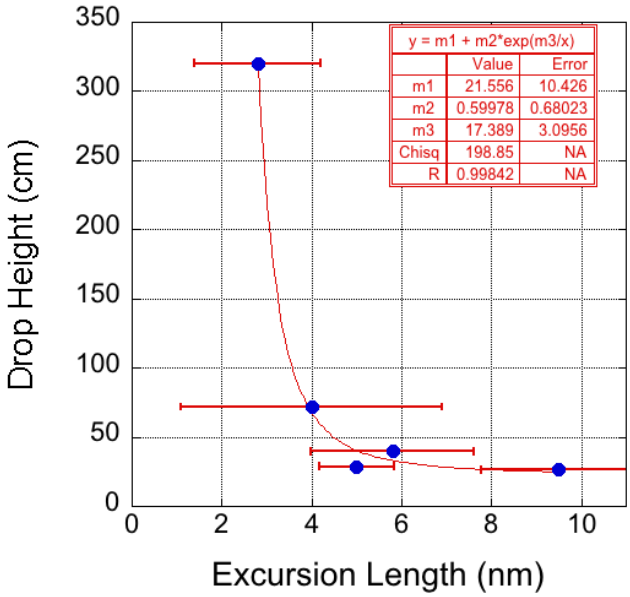

Figure 4.28. Average excursion length of each material verse H_{50}, error bars are given by the 95% confidence interval.

energy but not the length for this reason. The length verse drop height data was fit to an exponential equation of the form,

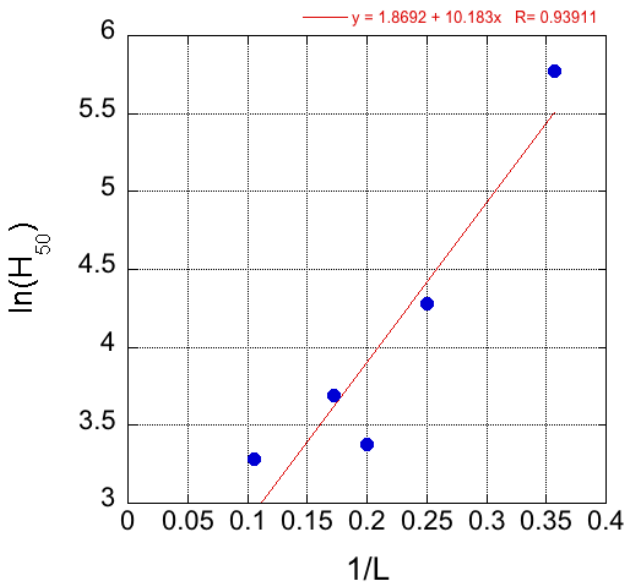

Figure 4.29. Excursion length data is linearized by plotting the natural log of the drop height verse the inverse of the excursion length.

$$H_{50} = A + B \exp\left(\frac{C}{L}\right) \tag{4.2}$$

with L being the excursion length. This equation along with the fitting parameters A, B, and C are also given in Figure 4.28. This fit has an R^2 value of 0.994, and could possibly be used to predict drop heights based on excursion length. This may be easier to see in the linearized plot shown in Figure 4.29 of the natural log of the drop height verse the inverse of the excursion length. At this point these proposed fits and parameters are purely empirical, there is not a mechanical reason this specific relationship was chosen. Further comparisons were also made between the shear stress and strain at yield and the drop height, however there was no observable correlation between any of these values. The total work done during indentation, equal to the entire area under the curve, also did not show and relation to the drop height.

While there seems to be evident trends of the initial pop-in with drop weight sensitivity, there are still many other factors that need to be taken into consideration. As mentioned factors like the size of particles can influence the drop weight sensitivity,

but in nanoindentation experiments size has no effect at all on measurements. Strain rates may also play a role, all the indents were performed at a single strain rate, if this were varied by changing the time or maximum load of the indent the pop-in phenomena maybe subject to change. Despite all these other influences it is a valuable insight that given the conditions and indentation parameters listed in these experiments there is a noticeable trend with H_{50} and initial pop-in length that can be described by the given curve fits of each plot. This could potentially be used as a quick, non-destructive method of determining a first order estimate of the drop weight sensitivity of new materials. As seen with ADAAF it would only be applicable to materials that displayed an elastic deformation behavior at low loads, alternative methods would need to devised for materials that behave similarly to ADAAF.

5. CHAPTER: CONCLUSION

Mechanical properties (hardness and modulus) were measured for aspirin and micron sized particles of six selected energetic materials. Table 5.1 at the end of the conclusion gives a comprehensive list of measured properties for all materials compared to literature values when available. Measurements made on aspirin show that the orientation of a Berkovich tip relative to the indentation surface can influence the measurement of properties by up to 8% in extreme cases. Nanoindentation results of RDX, HMX, and FOX-7 were compared to previous nanoindentation studies. It was found that the average property measurements on micron sized RDX, HMX, and FOX-7 were consistent with those previously reported for carefully grown, centimeter sized single crystals, despite the fact that previous measurements on FOX-7 were done with additives in the crystal structure and the RDX and HMX were subject to various additional mechanical processing. The hardness and modulus of TATB, ADAAF, and TNT/CL-20 are also experimentally measured and reported for the first time. In addition to the mechanical properties the yield behavior of each of these materials was characterized by the load and shear stress where the initial pop-in phenomena occurred, according the the Hertzian regime for elastic contact.

The length and energy of the initial pop-in was also used to compare with drop weight sensitivities of the energetic materials. This initial pop-in is usually attributed to the first signs of plastic deformation occurring in a material, indicating an elastic-plastic transition. It appears that a curve fit with the form of equation (4.2) can be used to empirically describe the relationship between the drop height and excursion length for materials that have a distinct elastic-plastic transition. This trend is also apparent with the energy or pop-ins however pseudo-elastic deformation introduces additional error, making the length a more reliable quantity for comparison. This

trend is supportive of both the dislocation pile-up and void collapse mechanisms for hot spot initiation during impact as the yield behavior is dependent on dislocation density and imperfections in the crystal. Materials with greater sensitivity may have a higher dislocation density (dislocation nucleation sources) or number of defects, that allow for greater pile-up, which makes the energy released in the elastic-plastic transition greater. This method cannot be applied to materials like ADAAF that behave plastically from the start of the indent with no rapid changes in displacement.

While general trends were identified there are many other factors not considered that would be needed in order to make an accurate direct comparison of mechanical properties to drop weight sensitivity. Another set of experiments could be used to do the same analysis at varying strain rates or with different tip geometries. Testing a larger number of materials would also be crucial in determining of the trends hold for a broader selection of materials, as was already seen this method of comparison did not work with ADAAF. Other samples that would be beneficial in testing would be PETN, CL-20, TNT, DAAF, cocrystals such as H_2O_2/CL-20, HMX/CL-20 and a wide selection of other energetic materials. If the trends hold out for a wide range of materials then this testing method could be used as an indicator of sensitivity in the early stages of energetic material synthesis as it requires a minimal amount of material and is a relatively quick test that can be easily standardized. The method for mounting crystals to measure the hardness and modulus can be used for any material that has well faceted surfaces large enough for indentation to be done on it. The smallest crystals mounted in this work were approximately 50μm in the longest dimension, which allowed for single or double indentations per crystal. This could prove useful in measuring the properties of materials that previously proved to be an experimental challege, as with the energetic cocrystals.

Table 5.1.
Comparison of Properties of Molecular Crystals

Material	Crystal Face*	H (GPa)	E_r (GPa)	τ_{avg} (GPa)
TATB	$(001)^a$	0.48	10.7	-
	Multiple	0.41	9.6	0.38
FOX-7	$(020)^b$	0.52	11.09	-
	$(\bar{1}01)^b$	0.63	16.65	-
	$(002)^b$	0.67	21.34	-
	Multiple	0.86	19.6	0.38
RDX	$(210)^c$	0.672	21.0	-
	$(001)^c$	0.615	16.2	-
	$(021)^c$	0.681	18.2	-
	$(210)^d$	0.798	22.9	-
	Multiple	0.74	19.1	0.39
HMX	$(010)^e$	1.13	23.18	-
	unknown^e	0.95	26.05	-
	$(010)^f$	0.65	17.6	-
	Multiple	0.99	24.5	0.83
ADAAF	Multiple	0.23	6.7	-
TNT/CL-20	Multiple	0.63	14.2	-
Aspirin	$(100)^g$	0.257	5.97	-
	$(001)^g$	0.240	9.57	-
	$(10\bar{2})^g$	0.152	4.96	-
	$(100)^h$	0.11-0.28	4.73-7.16	-
	$(001)^h$	0.11-0.14	2.81-3.11	-
	Multiple	0.32	7.2	0.95

*Multiple crystal faces indicate this work. ^{a} [57]. ^{b} [31]. ^{c} [48]. ^{d} [49]. ^{e} [55]. ^{f} [54]. ^{g} [24]. ^{h} [38].

REFERENCES

REFERENCES

[1] A. I. Kitaigorodsky. *Molecular Crystals and Molecules.* Academic Pressm, Inc (London) LTD., 1973.

[2] J. D. Wright. *Molecular Crystals (second edition).* Cambridge University Press, 1995.

[3] Wendy C. Duncan-Hewitt and George C. Weatherly. Evaluating the hardness, Young's modulus and fracture toughness of some pharmaceutical crystals using microindentation techniques. *J. Mater. Sci. Lett.*, 8:1350–1352, 1989.

[4] R. W. Armstrong and W. L. Elban. Materials science and technology aspects of energetic (explosive) materials. *Mater. Sci. Technol.*, 22(4):381–395, 2006.

[5] H. Kallmann and M. Pope. Photovoltaic effect in organic crystals. *J. Chem Phys.*, 30:585–586, 1959.

[6] V. Ramamurthy and K. Venkatesan. Photochemical reactions of organic crystals. *Chem. Rev.*, 87:433–481, 1987.

[7] E. Menard, V. Podzorov, S. H. Hur, A. Gaur, M. E. Gershenson, and J. A. Rogers. High-performance n- and p-type single-crystal organic transistors with free-space gate dielectrics. *Adv. Mater.*, 16(23-24):2097–2101, 2004.

[8] C. Y. Wu, O. M. Ruddy, A. C. Bentham, B. C. Hancock, S. M. Best, and J. A. Elliot. Modelling the mechanical behaviour of pharmaceutical powders during compaction. *Powder Technol.*, 152:107–117, 2005.

[9] C. Malla Reddy, G. Rama Krishna, and Soumyajit Ghosh. Mechanical properties of molecular crystals-applications to crystal engineering. *Cryst. Eng. Comm.*, 12:2296–2314, 2010.

[10] Francesca P. A. Fabbiani and Colin R. Pulham. High-pressure studies of pharmaceutical compouns and energetic materials. *Chem. Soc. Rev.*, 35:932–942, 2006.

[11] Louis J. Ignarro. After 130 years, the molecular mechanism of action of nictroglycerin is revealed. *Proc. Natl. Acad. Sci. USA*, 99(12):7816–7817, 2002.

[12] F. P. Bowden and Y. D. Yoffe. *Initiation and growth of explosion in liquids and solids.* Cambridge University Press, 1952.

[13] John B. Ramsay and Roger H. Goldie. *A working man's analysis of incidents and accidents with explosives at the Los Alamos National Laboratory, 1946-1997.* United States. Department of Energy, 1998.

[14] S. Ek. 6th symposium (international) on detonation. In *Sensitivity of explosive substances a multivariate approach*, pages 272–280, 1976.

[15] Jai Prakash Agrawal. *High Energy Materials: Propellants, Explosives and Pyrotechnics*. Wiley-VCH, 2010.

[16] Muhamed Suceska. *Test Methods for Explosives*. Springer, 1995.

[17] John E. Field, N. K. Bourne, S. J. P. Palmer, and S. M. Walley. Hot-spot ignition mechanisms for explosives and propellants. *Phil. Trans. R. Soc. Lond. A*, 339:269–283, 1992.

[18] R. W. Armstrong, C. S. Coffey, V. F. DeVost, and W. L. Elban. Crystal size dependence for impact initiation of cyclotrimethylenetrinitramine explosive. *J. Appl. Phys.*, 68(3):979–984, 1990.

[19] Xiao Lan Song, Yi Wang, Chong Wei An, Xiao De Guo, and Feng Sheng Li. Dependence of particle morphology and size on the mechanical sensitivity and thermal stability of octahydro-1,3,5,7-tetranitro1,3,5,7-tetrazocine. *J. Hazard. Mater.*, 159:222–229, 2008.

[20] Victor J. Belitto and Mikhail I. Melnik. Surface defects and their role in the shock sensitivity of cyclotrmethylene-trinitramine. *Appl. Surf. Sci*, 256:3478–3481, 2010.

[21] Xiang Min Liao and Timothe Scott Wiedmann. Measurement of process-dependent material properties of pharmaceutical solids by nanoindentation. *J. Pharm. Sci.*, 94(1):79–92, 2004.

[22] Yuan Yuan Jing, Yan Zhang, John Blendell, Marisol Koslowski, and M. Teresa Carvajal. Nanoindentation method to study slip planes in molecular crystals in a systematic manner. *Cryst. Growth. Des.*, 11:5260–5267, 2011.

[23] Christopher A. Schuh. Nanoindentation study of materials. *Mater. Today*, 9(5):32–40, 2006.

[24] Sunil Varughese, M. S. R. N. Kiran, Katarzyna A. Solanko, Andrew D. Bond, U. Ramamurty, and Gautam R. Desiraju. Interation anisotropy and shear instability of aspirin polymorphs established by nanoindentation. *Chem. Sci.*, 2:2236–2242, 2011.

[25] Xiao Dong Li, Dong Feng Diao, and Bharat Bhushan. Fracture mechanisms of thin amorphous carbon films in nanoindentation. *Acta Mater.*, 45(11):4453–4461, 1997.

[26] David F. Bahr, D. E. Kramer, and W. W. Gerberich. Non-linear deformation mechanisms during nanoindentation. *Acta Mater.*, 46(10):3605–3617, 1998.

[27] W. C. Oliver and G. M. Pharr. An improved technique for determining hardness and elastic modulus using load displacement sensing indentation experiments. *J. Mater. Res.*, 7(1564-1583), 1992.

[28] D. Lorenz, A. Zeckzer, U. Hilpert, and P. Grau. Pop-in effect as homogeneous nucleation of dislocations during nanoindentation. *Phys. Rev. B*, 67(172101), 2003.

[29] Michael R. Maughan and David F. Bahr. Dislocation activity under nanoscale contacts prior to discontinuous yield. *Mater. Res. Lett.*, 3(1):58–64, 2015.

[30] Z. H. Xu and X. Li. Effect of sample tilt on nanoindentation behaviour of materials. *Philos. Mag.*, 87(16):2299–2312, 2007.

[31] Xiao Qing Zhou, Zhi Peng Lu, Qi Zhang, Dong Chen, Hong Zhen Li, Fu De Nie, and Chao Yang Zhang. Mechanical anisotropy of the energetic crystal of 1,1-diamino-2,2-dinitroethylene (FOX-7): A study by nanoindentation experiemtns and density functional theory calculations. *J. Phys. Chem. C*, 120:13434–13443, 2016.

[32] R. H. B. Bouma, W. Duvalois, and A. E. D. M. Van Der Heijden. Microscopic characterization of defect structures in RDX crystals. *J. Microsc.*, 252(3):263–274, 2013.

[33] Kyle J. Ramos, David F. Bahr, and Daniel E. Hooks. Defect and surface asperity dependent yield during contact loading of an organic molecular single crystal. *Philos. Mag.*, 91(7-9):1276–1285, 2011.

[34] Victoria M. Masterson and Xiao Ping Cao. Evaluating particle hardness of pharmaceutical solids using AFM nanoindentation. *Int. J. Pharm.*, 362:163–171, 2008.

[35] Sunil Varughese, M. S. R. N. Kiran, Upadrasta Ramamurty, and Gautam R. Desiraju. Nanoindentation in crystal engineering: Quantifying mechanical properties of molecular crystals. *Angew. Chem. Int. Ed.*, 52:2701–2712, 2013.

[36] P. J. Wheatley. The crystal and molecular structure of aspirin. *J. Chem. Soc.*, pages 6036–6048, 1964.

[37] K. Ridgway, E. Shotton, and J. Glasby. The hardness and elastic modulus of some crystalline pharmaceutical materials. *J. Pharm. Pharmac.*, 21:19S–23S, 1969.

[38] D. Olusanmi, K. J. Roberts, M. Ghadiri, and Y. Ding. The breakage behaviour of aspirin under quasi-static indentation and single particle impact loading: Effect of crystallographic anisotropy. *Int. J. Pharm.*, pages 49–63, 2011.

[39] H. Mohammed, B. J. Briscoe, and K. G. Pitt. The intrinsic nature and the coherence of compacted pure pharmaceutical tablets. *Powder Technol.*, 165:11–21, 2006.

[40] Rahul V. Haware, Paul Kim, Lauren Ruffino, Brian Nimi, Catherine Fadrowsky, Michael Doyle, Stephan X. M. Boerrigter, Alberto Cuitino, and Ken Morris. Anisotropic crystal deformation measurements determined using powder x-ray diffraction and a new *in situ* compression stage. *Int. J. Pharm.*, pages 199–206, 2011.

[41] Michael R. Maughan, M. Teresa Carvajal, and David F. Bahr. Nanomechanical testing technique for millimeter-sized and smaller molecular crystals. *Int. J. Pharm.*, 486:324–330, 2015.

[42] Andrew Gouldstone, Krysten J. Van Vliet, and Subra Suresh. Simulation of defect nucleation in a crystal. *Nature*, 411:656, 2001.

[43] James R. Rice. Dislocation nucleation from a crack tip: An analysis based on the peierls concept. *J. Mech. Phys. Solids*, 40(2):239–271, 1992.

[44] H. W. Qiu, V. Stepanov, A. R. D. Stasio, T. M. Chou, and W. Y. Lee. Rdx-based nanocomposite microparticles for significantly reduced shock sensitivity. *J. Hazard. Mater.*, 185:489–493, 2011.

[45] John E. Field. Hot spot ignition mechanisms for explosives. *Acc. Chem. Res.*, 25:489–496, 1992.

[46] N. Mathew and R. C. Picu. Slip asymmetry in the molecular crystal cyclotrimethylenetrinitramine. *Chem. Phys. Lett.*, 582:78–81, 2013.

[47] Robert J. Hudson, Peter Zioupos, and Philip P. Gil. Investigating the mechanical properties of RDX crystals using nano-indentation. *Propellants Explos. Pyrotech.*, 37:191–197, 2012.

[48] Kyle J. Ramos, Daniel E. Hooks, and David F. Bahr. Direct observation of plasticity and quantitative hardness measurements in single crystal cyclotrimethylene trinitramine by nanoindentation. *Philos. Mag.*, 89(27):2381–2402, 2009.

[49] N. Scott Weingarten and Rosario C. Sausa. Nanomechanics of RDX single crystals by force-displacement measurements and molecular dynamics simulations. *J. Phys. Chem. A*, 119:9338–9351, 2015.

[50] Li Ma, Dylan J. Morris, Stefhanni L. Jennerjohn, David F. Bahr, and Lyle Levine. Finite element analysis and experimental investigation of the Hertzian assumption on the characterization of initial plastic yield. *J. Mater. Res.*, 24(3):1059–1068, 2009.

[51] James J. Haycraft, Lewis L. Stevens, and Craig J. Eckhardt. The elastic constants and related properties of the energetic material cyclotrimethylene trinitramine (RDX) determined by Brillouin scattering. *J. Chem. Phys.*, 124(024712), 2006.

[52] A. A. Zbib and David F. Bahr. Dislocation nucleation and source activation during nanoindentation yield points. *Metall. Mater. Trans. A*, 38A:2249–2255, 2007.

[53] Howard H. Cady, Allen C. Larson, and Don T. Cromer. The crystal structure of α-HMX and a refinement of the structure of β-HMX. *Acta Cryst.*, 16:617–623, 1963.

[54] S. O. Kucheyev, A. E. Gash, and T. Lorentz. Deformation and fracture of LLM-105 molecular crystals studied by nanoindentation. *Mater. Res. Express*, 2014.

[55] Ming Li, Wu Jun Tan, Bin Kang, Rui Juan Xu, and Wei Tang. The elastic modulus of β-HMX crystals determined by nanoindentation. *Propellants Explos. Pyrotech.*, 35:379–383, 2010.

[56] Howard H. Cady and Allen c. Larson. The crystal structure of 1,3,5-triamino-2,4,6-trinitrobenzene. *Acta Cryst.*, 18:485, 1965.

[57] N. Mathew and Thomas D. Sewell. Nanoindentation of the triclinic molecular crystal 1,3,5-triamino-2,4,6-trinitrobenzene: A molecular dynamics study. *J. Phys. Chem. C*, 120:8266–8277, 2016.

[58] Ulf Bemm and Henric Ostmark. 1,1-diamino-2,2-dinitroethylene: a novel energetic material with infinite layers in two dimensions. *Acta Cryst.*, pages 1997–1999, 1998.

[59] Jacqueline M. Veauthier, David E. Chavez, Bryce C. Tappan, and Damon A. Parrish. Synthesis and characterization of furazan energetics ADAAF and DOATF. *J. Energ. Mater*, 28:229–249, 2010.

[60] Chun Mei Zheng, Yu Ting Chu, Li Wen Xu, Feng Yun Wang, Wu Lei, Ming Zhu Xia, and Xue Dong Gong. Theoretical studeis on a new furazan compound bis[4-nitramino-furazanyl-3-azoxy]azofurazan (ADNAAF). *J. Mol. Model.*, 22:129, 2016.

[61] Shyam Karki, Tomislav Friscic, Laszlo Fabian, and Peter R. Laity. Improving mechanical properties of crystalline solids by cocrystal formation: New compressible forms of paracetamol. *Adv. Mater.*, 21:3905–3909, 2009.

[62] Daniel P. McNamara, Scott L. Childs, Jennifer Giordano, Anthony Iarriccia, James Cassidy, Manjunath S. Shet, Richard Mannion, Ed O'Donnell, and Aeri Park. Use of a glutaric acid cocrystal to improve oral bioavailability of a low solubility api. *Pharm. Res.*, 23:1888–1897, 2006.

[63] Chao Yang Zhang, Xiang Gui Xue, Yao Feng Cao, Jun Hong Zhou, An Bang Zhang, Hong Zhen Li, Yang Zhou, Rui Juan Xu, and Tao Gao. Towards low-sensitive and high-energetic co-crystal ii: structural, electronic and energetic features of CL-20 polymorphs and the observed CL-20-based energetic-energetic cocrystals. *Cryst. Eng. Comm.*, 16:5905–5916, 2014.

[64] Jie Heng Zhang and Jean'ne M. Shreeve. Time for pairing: cocrystal as advanced energetic materials. *Cryst. Eng. Comm.*, 18:6124–6133, 2016.

[65] Soumyajit Ghosh, Arobendo Mondal, M. S. R. N. Kiran, U. Ramamurty, and C. Malla Reddy. The role of weak interactions in the phase transition and distinct mechanical beavhior of two structurally similar caffeine co-crystal polymorphs studied by nanoindentation. *Cryst. Growth. Des.*, 13:4435–4441, 2013.

[66] Chandana Karunatilaka, Dejan-Kresimir Bucar, Lindsay R. Ditzler, Tomislav Friscic, Dale C. Swenson, Leonard R. MacGillivray, and Alexei V. Tivanski. Softening and hardening of macro- and nano-sized organic cocrystals in a single-crystal transformation. *Angew. Chem. Int. Ed.*, 50:8642–8646, 2011.

[67] De Zhou Guo, Qi An, III William A Goddard, Sergey V. Zybin, and Feng Lei Huang. Compressive shear reactive molecular dynamics studies indicating that cocrystals of TNT/CL-20 decrease sensitivity. *J. Phys. Chem. C*, 118:30202–30208, 2014.

[68] Hua Rong Li, Yuan Jie Shu, Shi Jie Gao, Ling Chen, Qing Ma, and Xue Hai Ju. Easy methods to study the smart energetic TNT/CL-20 co-crystal. *J. Mol. Model.*, 19:4909–4917, 2013.